Variability in fluid sources in the fluorite deposits from Asturias (N Spain): Further evidences from REE, radiogenic (Sr, Sm, Nd) and stable (S, C, O) isotope data

Virginia Sánchez [a,*], Esteve Cardellach [b], Mercé Corbella [b], Elena Vindel [a], Tomás Martín-Crespo [c], Adrian J. Boyce [d]

[a] Departamento de Cristalografía y Mineralogía, Facultad de Ciencias Geológicas, Universidad Complutense, 28040, Madrid, Spain
[b] Departament de Geologia, Facultat de Ciences, Universitat Autònoma, Bellaterra, 08193 Barcelona, Spain
[c] ESCET, E. Departamental II, Universidad Rey Juan Carlos, Móstoles, 28933, Madrid, Spain
[d] Scottish Universities Environmental Research Centre (SUERC), East Kilbride, Glasgow G75 0QF, Scotland, UK

Keywords:
Fluorite
Sr isotopes
Sm–Nd isochron
Stable isotopes
Asturias
Spain

A B S T R A C T

Fluorite deposits in Asturias (Iberian Peninsula, N Spain) are hosted in Permo-Triassic and Paleozoic rocks. The three main districts of Berbes, La Collada and Villabona preferentially occur along the margins of a Mesozoic basin and comprise veins and stratabound mineralization composed of fluorite, barite, calcite, dolomite, quartz and sulphides. Although the geological framework is similar and fluorite dominates in all deposits, variability in sources and processes has led to each area having its own distinctive characteristics. Sr isotope data of fluorite, calcite and barite ($^{87}Sr/^{86}Sr = 0.7080$ to 0.7105) are compatible with a mixing between seawater and an evolved groundwater that interacted with basement rocks. Sm/Nd ratios in fluorites from Villabona district provide an isochron age of 185 ± 28 Ma (Late Triassic–Late Jurassic), consistent with other hydrothermal events in the Iberian Peninsula and Europe. The total REE content of fluorite increases from Berbes to Villabona by an order of magnitude (0.4 to 9.3). The La/Lu ratio in fluorites decreases from a mean value of 0.36 in Berbes, 0.17 in La Collada to 0.09 in Villabona indicating a strong fractionation between LREE and HREE.

Calculated $\delta^{18}O$ of fluids ranges from 0.3 to +7.4‰ during barite precipitation, from +0.8 to +4‰ during quartz formation and around +3‰ during carbonate deposition. The $\delta^{34}S$ of barite (+17 to +56‰), is explained by sulphate reduction processes (either thermochemically or bacterially mediated) in a system closed with respect to sulphate. The $\delta^{34}S$ of sulphide (+0.6 to −32‰) is compatible with these processes although bacterial processes must have dominated at Villabona. Organic matter was an important source of C in the fluids especially in Villabona ($\delta^{13}C = -14.8$ to −2.5‰ in calcites and from −7.9 to −2.2‰ in dolomites). Differences in host rock and position within the basin, and the lithology of the basement, seem to have exerted a strong control on the chemistry of mineralizing fluids providing each district with distinctive characteristics.

1. Introduction

Asturias is one of the most important fluorite producing regions in Europe. Mining started in the 1930's, with the most important activity in the 1960's. More than 15 Mt. of ore has been produced and mining continues today. The most important active deposits are found in three districts: Berbes, La Collada and Villabona (Fig. 1). Mineralization is typically fluorite-rich and sulphide-poor and shares characteristics with MVT deposits. Similar examples are found widespread in Europe, e.g., the Massif Central of France (Sizaret et al., 2004; Munoz et al., 2005), the Hercynian massifs of Germany (Behr et al., 1987; Behr and Gerler, 1987; Lüders and Möller, 1992; Schwinn et al., 2006), Spain (Canals and Cardellach, 1993; Galindo et al., 1994; Tornos et al., 2000; Cardellach et al., 2007; Piqué et al., 2008) and the Northern Pennines in England (Sawkins, 1966; Dunham, 1988; Cann and Banks, 2001).

The deposits preferentially occur along the margins of a Mesozoic basin which unconformably overlies Paleozoic and Precambrian basement rocks. Fluorite mineralization occurs as vein and stratabound bodies in highly silicified Permo-Triassic red-bed sediments (marls and sandstones) and carbonates, and as veins within limestones of the Paleozoic basement. Previous studies focused on the geological, mineralogical and geochemical (fluid inclusion studies) aspects of these mineralizations (García Iglesias and Touray, 1976, 1977; García Iglesias, 1978; Loredo and Garcia Iglesias, 1984; García Iglesias and Loredo, 1992, 1994). García Iglesias and Loredo (1994) suggested that a possible source of F is the volcanic rocks (trachyandesites) outcropping in the depocenter of the Permo-

* Corresponding author. Tel.: +34 913944868; fax: +34 913944872.
E-mail address: visanche@geo.ucm.es (V. Sánchez).

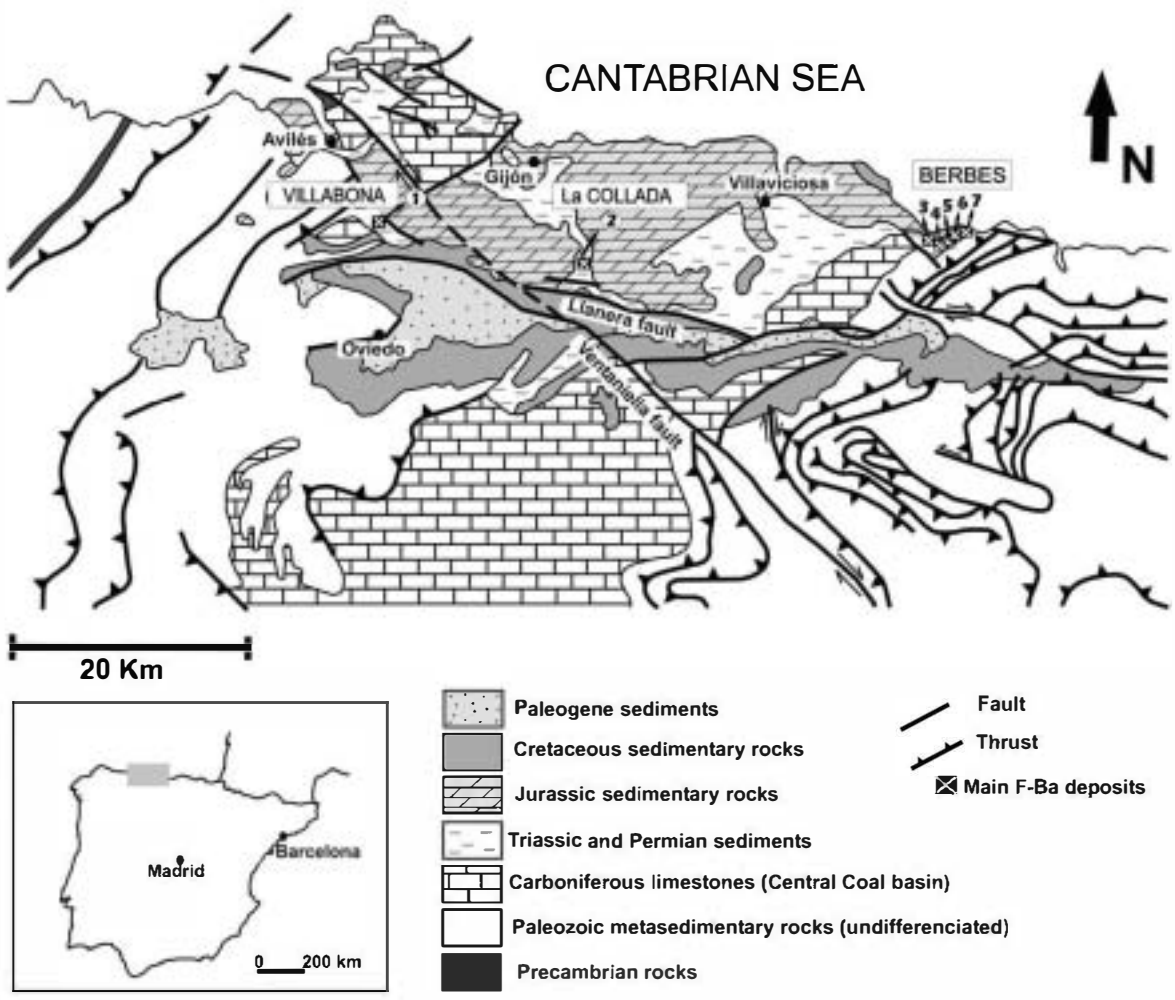

Fig. 1. Simplified map showing the location of the fluorite deposits and main districts: (1) Moscona Mine, (2) La Viesca Mine, (3) Emilio Mine, (4) Valnegro, (5) San Lino, (6) Aurora Vein and (7) La Paredona. (Modified from Sánchez et al., 2009).

Triassic basin, near Villaviciosa (Fig. 1). Recent fluid inclusion studies (Sánchez et al., 2009) concluded that precipitation of fluorite was caused by mixing between H_2O–NaCl–$CaCl_2$ brines (salinities from 7 to 13 wt.% NaCl equiv. and 11 to 14 wt.% $CaCl_2$ equiv.) and lower salinity H_2O–NaCl fluids (from 0 to 8 wt.% NaCl equiv.) at temperatures between 80 and 170 °C. The metal content of the fluids was as high as 160 to 500 ppm Zn, 90 to 170 ppm Pb and 320 to 480 ppm Ba (Sánchez et al., 2009) in the high salinity fluid. A decrease of T_h of the fluids and their metal content from the E (Berbes and La Collada; mode values: 140 to 120 °C) to the W (Villabona, mode: 90 °C) was also reported (Sánchez et al., 2009).

However, the information about the fluid sources was limited. In this paper we present data on the rare earth element (REE) concentrations and Sr and Sm–Nd isotope ratios of fluorite, together with stable isotope data from gangue minerals (sulphides, sulphates, carbonates and quartz) in order to shed further light on the origin of key components of the mineralizing system. Specifically, REE data are useful to gather information about the source of these elements and migration processes as well as the chemical composition of the fluid (Möller et al., 1984). Sr isotopes of fluorite and hydrothermal carbonates are helpful in identifying the solute sources and fluid paths, whereas we use Sm–Nd isotope ratios of the fluorites to place broad constraints on the age of mineralization. Finally, the stable isotope (S, C and O) study elucidates the origin of the fluids responsible for, and the mechanisms of gangue mineral deposition whose relationship with the fluorite mineralization is well understood.

2. Geological setting

The study area (Fig. 1) is constituted by Mesozoic rocks (Triassic to Jurassic), unconformably overlying Paleozoic basement which was folded and faulted during the Carboniferous Variscan orogeny. The Paleozoic rocks consist of Cambrian limestones and sandstones, Ordovician and Devonian quartzites and alternating carbonate and siliciclastic Carboniferous sediments.

Post-Variscan deformational events started with extension that led to the development of the Permo-Triassic basins that were filled up with red clays, evaporites, and calcarenites. Some lava flows and pyroclastic rocks of basaltic to trachyandesitic composition (Valverde, 1993) crop out interbedded within Permo-Triassic red sediments. The second major extensional period took place during the Upper Jurassic and Lower Cretaceous, which was related to the opening of the Bay of Biscay producing the regionally most important Mesozoic basins. Limestone and detrital sediment deposition dominated this event. The Variscan basement and the Mesozoic cover were both subsequently deformed during the Alpine orogeny.

Furthest East, in the Berbes area (Fig. 1), two styles of mineralization are found: veins (i.e. Aurora mine, now abandoned) hosted in Carboniferous limestones (Namurian) and stratabound (Emilio mine, active), within a silicified Permo-Triassic conglomeratic breccia that lies unconformably over the Carboniferous limestones (Sánchez de la Torre et al., 1977; Tejerina and Zorrilla, 1980; Fernández, 1995). The breccia is composed of a variety of Carboniferous carbonate fragments, and its greatest thickness is found in areas

close to faults affecting the basement. Fluorite fills cm- to meter-thick veins and dissolution cavities and replaces some clasts. The mineralization terminates abruptly where the breccia grades into marls and sandstones (Fig. 2A).

Mineralization in La Collada district (Fig. 2B) is similar to Berbes. In La Viesca mine (active) fluorite is present as vein and stratabound bodies hosted in Permo-Triassic rocks unconformably overlying the Paleozoic basement. Veins dominate over breccia replacements and ore grades decrease towards the Permo-Triassic marls, in the upper parts of the formation.

Furthest west, the Villabona district (Fig. 1) hosts the most productive and active fluorspar deposit in the region: the Moscona mine. The mineralization also consists of replacement (stratabound) and vein bodies (Fig. 2C). Stratabound fluorite is hosted by a 2 to 12 m thick silicified carbonate bed, but current production comes mainly from veins related to normal faults cross-cutting the Permo-Triassic strata. The basement rocks in Moscona comprise Devonian shales, sandstones and limestones. However, 4 km to the south, at the old mine of Villabona, the Permo-Triassic rocks lie unconformably over Carboniferous basement, which contain coal seams (Stephanian).

Permo-Triassic rocks are overlain by Jurassic limestones, which thin towards the W of the region. The outcropping Mesozoic sediments depict an E–W basin, bounded by faults in its northern and southern margins. According to this distribution, facies types and sedimentological record in the three studied areas, Moscona mine would be located close to the southwestern margin of the Mesozoic basin, which would have its depocenter in the Villaviciosa area (see Fig. 1), where the volcanic rocks crop out, whereas La Collada and Berbes districts would be situated in the Southern and Eastern margins, respectively, of the Mesozoic basin.

3. Mineralogy and paragenesis

The mineralogy of the deposits is simple and comprises fluorite, quartz, barite, calcite, dolomite and minor sulphides (pyrite, marcasite, galena and chalcopyrite). Fluorite precipitation was preceded by widespread silicification (Q1 in Fig. 3) and local chloritization of the host rocks. Fluorite displays distinct colours: from dominantly purple in Berbes, blue or purple in La Collada, to yellow in Villabona, although colourless, blue and green varieties are common. Pyrite and chalcopyrite crystals are found either trapped in or growing over fluorite. A second generation of quartz crystals (Q2) precipitated coevally and after fluorite and was followed by carbonate. Calcite is abundant in all districts: a first generation grew as euhedral crystals over fluorite in Berbes and La Collada (CC1) and a late calcite (CC2), especially abundant in La Collada and Villabona, forms scalenohedrons. Saddle dolomite is also found, in minor amounts, in these districts.

Barite and quartz were the last phases to precipitate. Barite is abundant in the Berbes area, where occasionally it constitutes monomineralic veins (BA1). A later generation of barite (BA2) was only recognized in Villabona, with crystals having a characteristic pale blue colour. Late quartz crystals (Q3) are typically idiomorphic (Herkimer diamond-type) and contain large hydrocarbon-bearing inclusions (Arcos and Tornos, 1997), commonly visible to the naked eye. Q3 quartz has only been found in the Berbes district, but hydrocarbon-bearing fluid inclusions have been also recognized in fluorite (García Iglesias and Touray, 1976). Moreover, bitumen is found associated with marcasite, calcite and late barite, especially in Emilio mine (Berbes area).

The abundance of gangue minerals, especially barite and sulphides, is irregular at both deposit and district scales. In Villabona (Moscona mine) sulphides (pyrite and marcasite) and barite are particularly abundant in the northern part. Sulphides are also present in La Collada and Berbes although in lesser amounts. Barite is scarce in La Collada and, at a regional scale it seems to be more abundant in the east.

4. Samples and methods

For this study, samples of fluorite, quartz, marcasite, pyrite, calcite, dolomite and barite from the three active mines, namely Emilio (Berbes), La Viesca (La Collada) and Moscona (Villabona) have been analyzed. REE concentrations were analyzed in 15 samples of fluorite and two samples of Permo-Triassic volcanic rocks (Villaviciosa) from the only outcrop available close to the mineralization area, a possible source of fluoride as suggested by García Iglesias and Loredo (1994). Analyses were performed at ACTLABS, Canada, by ICP-MS. Results were normalized to the Post-Archaean Australian Shale (PAAS) after McLennan (1989).

$^{87}Sr/^{86}Sr$ isotopic compositions were determined for 27 fluorites and 15 calcites from all three areas and 7 barite and 2 dolomite samples from Berbes and Villabona. Sm–Nd isotopes were measured in 14 samples of fluorite of different colours (yellow, purple, blue and colourless) from the three districts, in the hope that colour changes may reflect variations in Sm/Nd ratios and allow calculation of an isochron age (Chesley et al., 1994). $^{87}Sr/^{86}Sr$ and Sm–Nd analyses were performed at the Geochronology and Isotope Geochemistry Laboratory (Universidad Complutense, Madrid, Spain). Fluorite samples were leached with 12 ml 6 N HCl and then spiked with a mixed tracer ^{149}Sm–^{145}Nd. Barite separates were leached once with 5 ml 6 N HCl and calcite with 5 ml 2.5 N HCl. Fluorite and barite separates were reheated at 120 °C for one week in order to achieve isotopic equilibration. The sample solutions were dried down and converted to chlorides for complete dissolution and re-equilibration. Samples were passed through a large (Dowex AG-50W-X12, 200-40) cation-exchange resin separating Sr and REE. Sm was separated from Nd using cation-exchange (Dowex AG-50W-X12, 200-40) resin (Richard et al., 1976). Both Sm and Nd were loaded with dilute H_3PO_4 acid onto tantalum filaments in respectively the single or triple filament mode run on an automated multicollector VG sector 54 mass spectrometer. Isotopic ratios corrected for blank and mass fractionation, $^{143}Nd/^{144}Nd$ data are normalized to $^{146}Nd/^{144}Nd = 0.7219$ and adjusted to JNdi-1 $^{143}Nd/^{144}Nd = 0.512113 \pm 0.00002$ (2σ, $n = 8$) and La Jolla standard $^{143}Nd/^{144}Nd = 0.511860 \pm 0.00002$ (2σ, $n = 7$). Isochron ages were calculated using the ISOPLOT programme of Ludwig (1998). The εNd values (the deviation in parts per 10^4 from coeval bulk earth) were calculated using present day values for bulk earth of $^{143}Nd/^{144}Nd$ of 0.512636 and $^{147}Sm/^{144}Nd$ of 0.1967. $^{87}Sr/^{86}Sr$ data are normalized to $^{88}Sr/^{86}Sr = 0.1194$ and adjusted to NBS 987 standard. The mean value of $^{87}Sr/^{86}Sr$ for 11 analysis of the Sr standard was $^{87}Sr/^{86}Sr = 0.710244 \pm 0.00003$ (2σ).

Carbon ($\delta^{13}C$) and oxygen ($\delta^{18}O$) isotopic compositions were analyzed in 30 samples of calcite from the three deposits and 4 dolomite samples from Berbes and Villabona, following the method of McCrea (1950). Analytical work was done on a Finnigan MAT250 mass spectrometer at the Scientific Technical Services (Universitat de Barcelona, Spain). C and O isotope compositions are reported in the conventional δ notation as per mil (‰) deviations relative to V-PDB and V-SMOW, respectively.

Eight quartz separates from Berbes and 1 from La Collada were analyzed for $^{18}O/^{16}O$ at the Stable Isotope Laboratory in the SUERC (East Kilbride, Glasgow, UK) using a laser fluorination procedure, involving total sample reaction with excess ClF_3 using a CO_2 laser as a heat source (in excess of 1500 °C; following Sharp, 1990). This O_2 was then converted to CO_2 by reaction with hot graphite, then analyzed on-line by a VG SIRA 10 spectrometer. Reproducibility is better than ± 0.3‰ (1σ), based on repeat analyses of internal and international standards during sample runs. Results are reported in standard notation ($\delta^{18}O$) as per mil (‰) deviations from the V-SMOW standard.

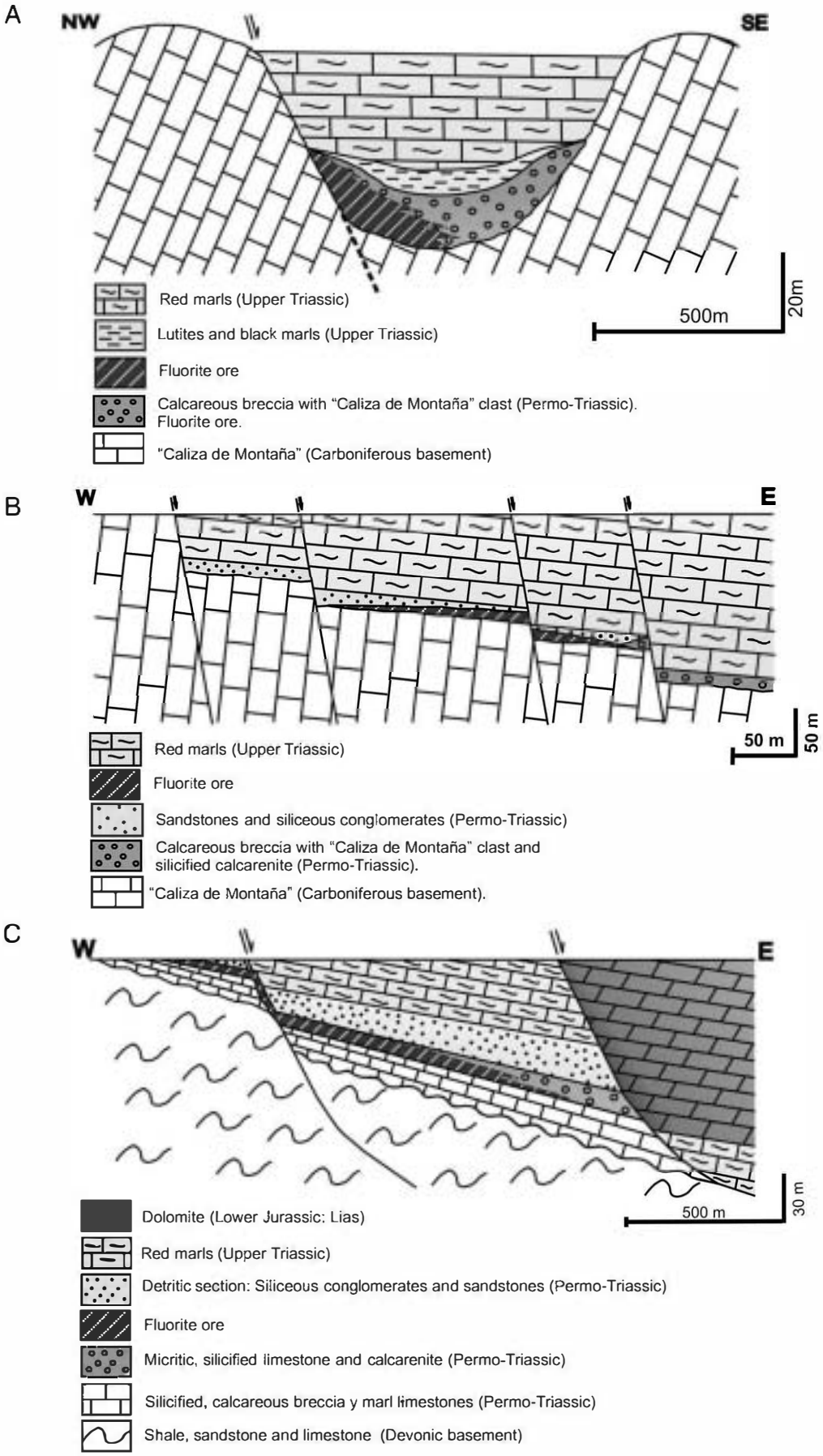

Fig. 2. Simplified cross-sections of fluorite deposits (A) Emilio Mine, Berbes district, (B) La Viesca Mine, La Collada district, and (C) Moscona Mine, Villabona district.

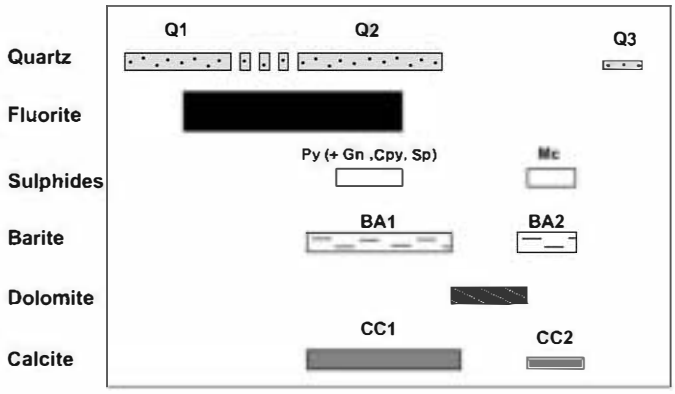

Fig. 3. Paragenetic sequence in Asturias deposits. (Modified from Sánchez et al., 2005).

Sulphur isotope analyses were performed on 28 barites from Berbes and Villabona and on 16 sulphides (marcasite, pyrite and galena) from the three areas. Sulphides were analyzed by standard techniques (Robinson and Kusakabe, 1975) in which SO_2 gas was liberated by combusting with excess Cu_2O at 1075 °C, *in vacuo*. Barite analyses were performed by the technique of Coleman and Moore (1978), in which SO_2 gas is liberated by combustion with excess Cu_2O and silica, at 1125 °C. Liberated gases were analyzed on a VG Isotech SIRA II mass spectrometer, and standard corrections applied to raw $\delta^{66}SO_2$ values to produce true $\delta^{34}S$. The standards employed were the international standards NBS-123 and IAEA-S-3, and the SUERC standard CP-1. These gave $\delta^{34}S$ values of +17.1‰, −31.5‰ and −4.6‰ respectively, with 1σ reproducibility better than ±0.2‰. Data are reported in $\delta^{34}S$ notation as per mil (‰) variations from the Vienna Canyon Diablo Troilite (V-CDT) standard. The analyses of 9 barites and 10 sulphides were performed at the Scottish Universities Environmental Research Centre. The other 19 barite and 6 sulphide samples were analyzed for the sulphur isotopic composition using an on-line elemental analyzer (EA) continuous flow isotope ratio mass spectrometer (IRMS). Isotope ratios were calculated using the NBS-127, IAEA-S-1 and IAEA-S-3 standards and are reported as permil (‰) deviation relative to the V-CDT standard. The precision was better than ±0.1‰. The same technique was used to analyze the O isotopic composition of barite samples. Results are reported as permil deviation respect to the V-SMOW standard. Analyses were performed at the Serveis Cientificotècnics of the Universitat de Barcelona (Spain).

5. Results

5.1. Rare earth elements

Fluorites from the three deposits show significant differences in terms of REE concentrations and distribution (Table 1). Total REE concentrations (ΣREE) are low, with mean values of 0.4 ppm in Berbes, 1.1 ppm in Collada and 9.3 ppm in Villabona, showing an increase in ΣREE of an order of magnitude from east to west. Yellow fluorite, exclusively found in Villabona, is characterized by higher REE concentrations than purple, blue and colourless fluorite (Berbes and La Collada). The volcanic rocks of Permian age (trachyandesite) show higher ΣREE content (13.7 ppm) than the fluorites.

The distribution ofREE in fluorites shows convex-up patterns with a slight enrichment of the MREE (Middle REE) more pronounced in Berbes and La Collada, and no Eu anomalies. A positive Ce anomaly in fluorites from Berbes is observed, contrasting with fluorites from La Collada and Villabona. The REE distribution in Permian trachyandesites depicts an almost flat pattern with a minor positive Eu anomaly (Fig. 4).

Fractionation between REE may be recognized through the La/Ho and La/Lu ratios. La/Ho ratios give a measure of fractionation between LREE (Light REE) and MREE whereas La/Lu (or La/Yb) ratios show the fractionation between LREE and HREE (Heavy REE). The La/Ho mean ratios vary from 0.095 in Berbes, 0.025 in La Collada to 0.033 in Villabona whereas the La/Lu ratio decreases from a mean value of 0.36 in Berbes and 0.17 in La Collada to 0.09 in Villabona (see Table 1), revealing a decrease in the relative concentration of LREE from E to W. The mean La/Yb ratio of each district, that is, the degree of fractionation between HREE and LREE, also decreases from E to W: Berbes shows a large La/Yb range compared to the other two districts and the highest mean La/Yb ratio (0.29), whereas Villabona has the lowest values for La/Yb mean ratios (0.06) and La Collada presents an intermediate value (0.09).

Table 1
REE, Rb and Sr concentrations in fluorite (ppm).

District	Berbes					Collada					Villabona					Volc. rock Permotrias.		PAAS
Colour	Cl	P	Cl	Cl	Cl	Cl	P	B	B	B	Y	Y	Y	Y	P			
Sample	BE03-03	BE03-04	BE03-36	BE05-07	BE05-20	CO04-03	CO04-03	CO04-04	CO04-06	CO04-10	VI04-07	VI04-10	VI04-15	VI04-19	VI04-19	VI04-18-1	VI04-18-2	
La	0.002	0.003	0.003	0.001	0.001	0.001	0.003	0.003	0.002	0.004	0.032	0.047	0.026	0.023	0.029	0.908	0.984	38.20
Ce	0.005	0.008	0.010	0.005	0.004	0.005	0.010	0.008	0.006	0.008	0.063	0.074	0.050	0.044	0.051	0.874	0.957	79.60
Pr	0.002	0.006	0.010	0.003	0.002	0.006	0.019	0.017	0.008	0.012	0.119	0.122	0.097	0.093	0.084	0.925	0.988	8.830
Nd	0.003	0.009	0.014	0.006	0.007	0.008	0.041	0.040	0.012	0.020	0.218	0.211	0.202	0.191	0.142	0.903	0.956	5.550
Sm	0.004	0.016	0.023	0.013	0.027	0.018	0.151	0.164	0.027	0.043	0.551	0.515	0.578	0.553	0.270	1.150	1.200	33.90
Eu	0.008	0.020	0.025	0.012	0.109	0.022	0.204	0.239	0.057	0.057	0.914	0.839	1.000	0.906	0.426	1.694	1.722	1.080
Gd	0.011	0.026	0.054	0.024	0.090	0.036	0.326	0.412	0.075	0.092	1.260	1.107	1.320	1.253	0.541	1.127	1.144	4.660
Tb	0.013	0.026	0.065	0.026	0.103	0.039	0.284	0.375	0.090	0.090	1.447	1.253	1.525	1.382	0.568	0.956	0.982	0.774
Dy	0.009	0.030	0.066	0.028	0.107	0.047	0.218	0.314	0.096	0.096	1.509	1.256	1.585	1.464	0.536	0.870	0.908	4.680
Ho	0.010	0.020	0.061	0.030	0.101	0.040	0.161	0.252	0.091	0.091	1.302	1.070	1.382	1.282	0.474	0.787	0.797	0.991
Er	0.008	0.019	0.062	0.031	0.101	0.043	0.136	0.205	0.085	0.093	1.275	1.101	1.388	1.194	0.461	0.891	0.880	2.850
Tm	0.012	0.012	0.030	0.020	0.062	0.020	0.072	0.116	0.054	0.059	0.963	0.886	1.136	0.928	0.343	0.847	0.840	0.405
Yb	0.004	0.007	0.014	0.011	0.035	0.011	0.035	0.067	0.028	0.032	0.638	0.603	0.798	0.663	0.227	0.784	0.791	2.820
Lu	0.005	0.005	0.009	0.005	0.021	0.007	0.014	0.028	0.014	0.021	0.457	0.439	0.577	0.464	0.171	0.783	0.783	0.433
ΣREE	0.096	0.207	0.446	0.215	0.77	0.303	1.674	2.24	0.658	0.718	10.75	9.523	11.66	10.44	4.323	13.50	13.93	184.77
La/Lu	0.51	0.62	0.31	0.28	0.06	0.19	0.21	0.11	0.15	0.18	0.07	0.011	0.04	0.05	0.17	1.16	1.29	
La/Ho	0.2	0.15	0.049	0.033	0.0099	0.025	0.018	0.012	0.002	0.044	0.024	0.044	0.019	0.018	0.06	1.15	1.23	
La/Yb	0.4	0.43	0.21	0.09	0.028	0.09	0.085	0.044	0.07	0.125	0.05	0.07	0.03	0.034	0.127	1.16	1.24	
Rb	<1	<1	<1	<1	<1	<1	<1	<1	<1	<1	<1	<1	<1	<1	<1	126	127	
Sr	24	27	17	32	59	24	41	29	18	16	55	77	50	44	29	–	–	

PAAS: Post-Archaean Australian Shales.
Cl: colourless fluorite, P: purple fluorite, B: blue fluorite, and Y: yellow fluorite.

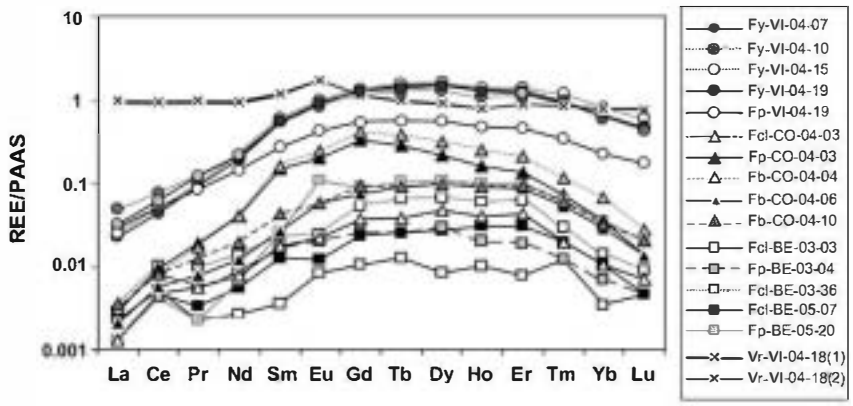

Fig. 4. REE distribution patterns of fluorite samples from Villabona (VI), Collada (CO) and Berbes (BE) district. All samples are normalized to the Post-Archaean Australian Shale (PAAS). Fcl: colourless fluorite, Fp: purple fluorite, Fb: blue fluorite, Fy: yellow fluorite, Vr: volcanic rock.

5.2. Sm–Nd

Yellow, purple and colourless fluorite separates from the three deposits were selected for analysis of Nd isotopes. Sm and Nd concentrations are quite variable among the deposits (Table 2). There is a clear relationship between the Sm and Nd content and the colour of fluorite. Purple fluorite, scarce in the Villabona deposit, shows lower values than yellow fluorite. In fluorites from Berbes and La Collada, Sm and Nd concentrations are low: from 0.08 to 1.91 ppm and from 0.7 to 2.49 ppm for Sm and Nd respectively (Berbes) and from 0.21 to 1.91 ppm and from 0.51 to 1.35 ppm for Sm and Nd respectively (La Collada). These concentrations contrast with those in fluorites from Villabona: Sm from 1.68 to 3.71 ppm and Nd from 4.70 to 8.90 ppm. Sm and Nd concentrations in yellow fluorite from Villabona are high and variable enough to obtain a reliable isochron. In a $^{143}Nd/^{144}Nd$ vs. $^{147}Sm/^{144}Nd$ plot (Fig. 5) the fluorite from Villabona depicts an isochron corresponding to an age of 185 ± 28 Ma (MSWD=0.3), that is, Late Triassic to Late Jurassic, with an initial $^{143}Nd/^{144}Nd$ of 0.511911 ± 0.000054. The calculated εNd values at 185 Ma are fairly uniform and range from -9.8 to -9.3.

5.3. Rb–Sr

52 samples of fluorite, calcite, dolomite and barite were analyzed for their Sr isotope composition (Table 3; Fig. 6). Berbes (0.7080 to 0.7097) and La Collada (0.7088 to 0.7105) show relatively large variations in $^{87}Sr/^{86}Sr$ in contrast, in Villabona Sr isotope values are more homogeneous (0.7082 to 0.7088). The observed $^{87}Sr/^{86}Sr$ ranges do not seem to depend on the analyzed mineral although in Berbes calcite shows slightly higher ratios than fluorite and at La Collada, calcite is slightly less radiogenic. Rb concentrations in fluorites are lower than 1 ppm (detection limit of the analytical method) whereas Sr ranges from 16 to 77 ppm (see Table 1). A trachyandesite interbedded within sediments of Permo-Triassic age has $^{87}Sr/^{86}Sr$ ratio of 0.7118 and $^{87}Rb/^{86}Sr$ ratio of 1.491 (see Table 4). The calculated $^{87}Sr/^{86}Sr$ ratio of these rocks at the time of fluorite mineralization ranges from 0.7073 and 0.7085 for ages of 213 and 157 Ma, respectively, values that are similar or lower than the range obtained for the ore and gangue minerals (0.7080 to 0.7110). $^{87}Sr/^{86}Sr$ ratio of seawater from Late Triassic to Late Jurassic ranged from 0.7075 to 0.7070 (Burke et al., 1982).

5.4. Stable isotopes

5.4.1. Carbonates

The $\delta^{13}C$ values for both generations of calcites from Berbes and La Collada are similar and range from 0.7 to +6.1‰ and a sample of dolomite gave a value of +3.2‰ (Table 5). However, the $\delta^{13}C$ values of carbonates from Villabona are distinctly lower, ranging from −14.8 to −2.5‰ in calcite and from −7.9 to −2.2‰ in dolomite (Table 5). The $\delta^{18}O$ of hydrothermal calcite (CC1 and CC2) ranges from +17.4 to +24.1‰, with no significant differences between the deposits, despite representing two distinct generations (Fig. 3). The $\delta^{18}O$ of saddle dolomite ranges from +22 to +22.7‰.

5.4.2. Quartz

All samples of Q2 and Q3 are isotopically heavy (Table 6). Q2 from Berbes have $\delta^{18}O$ ranging from +19.3 to 22.4‰ ($n=5$) and a sample from La Collada gave a value of +20.8‰. Q3 quartz shows more homogeneous values: +23.0 to +23.5‰ ($n=3$).

Table 2
Sm–Nd analytical data for fluorite from Villabona, Berbes and La Collada districts. εNd values are calculated using an age of 185 Ma. Present day $(^{143}Nd/^{144}Nd)_{CHUR}=0.512636$ and $(^{147}Sm/^{144}Nd)_{CHUR}=0.1967$; *CHUR* chondritic uniform reservoir.

District	Sample no.	Mineral	Sm (ppm)	Nd (ppm)	Sm/Nd	$^{147}Sm/^{144}Nd$	$^{143}Nd/^{144}Nd$	$^{143}Nd/^{144}Nd$ err abs	εNd_{185}
Villabona	VI-04-07	Yellow fluorite	2.09	4.70	0.4447	0.2688	0.512223	0.00003	−9.8
	VI-04-10	Yellow fluorite	3.30	8.90	0.3708	0.2241	0.512186	0.00003	−9.5
	VI-04-14	Yellow fluorite	3.71	5.89	0.629	0.3802	0.512379	0.00003	−9.3
	VI-04-15	Yellow fluorite	3.45	6.60	0.5227	0.3160	0.512300	0.00003	−9.4
	VI-04-19A	Yellow fluorite	3.58	6.25	0.5728	0.3463	0.512324	0.00006	−9.6
	VI-04-19M	Purple fluorite	1.68	5.39	0.3117	0.1884	0.512141	0.00004	−9.6
Berbes	BE-03-32	Blue fluorite	0.87	1.74	0.5	–	–	–	–
	BE-03-36	Colourless fluorite	0.08	0.7	0.1143	–	–	–	–
	BE-03-38	Colourless fluorite	0.81	1.78	0.4551	–	–	–	–
	BE-03-39	Colourless fluorite	0.28	0.94	0.2979	–	–	–	–
	BE-03-51	Purple fluorite	1.91	2.49	0.7671	–	–	–	–
La Collada	CO-04-06B	Blue fluorite	0.21	0.51	0.417	–	–	–	–
	CO-04-06A	Blue fluorite	0.27	0.54	0.497	–	–	–	–
	CO-04-03A	Blue fluorite	0.9	1.35	0.661	–	–	–	–

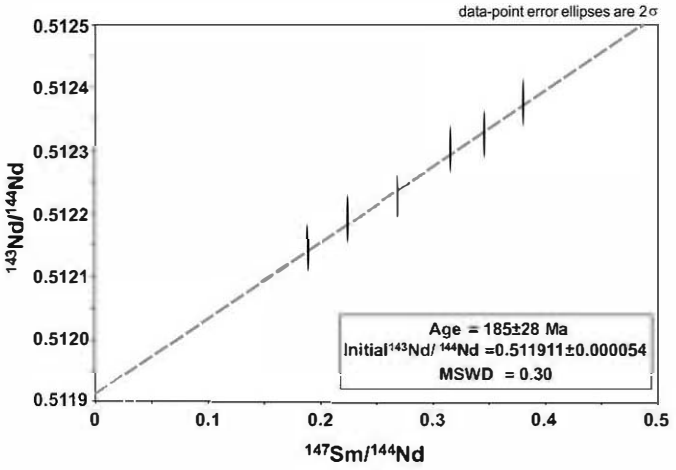

Fig. 5. Sm–Nd isochron diagram for fluorite samples from Villabona district (Asturias, Spain).

Table 3
$^{87}Sr/^{86}Sr$ isotope data for fluorite, calcite and barite from Berbes, La Collada and Villabona districts.

District	Sample	Mineral	$^{87}Sr/^{86}Sr$	$^{87}Sr/^{86}Sr$ (abs err)
Berbes	BE-03-03	Fluorite	0.709509	0.00004
	BE-03-36	Fluorite	0.708018	0.00006
	BE-03-38	Fluorite	0.708652	0.00005
	BE-03-39	Fluorite	0.708717	0.00006
	BE-03-51	Fluorite	0.708731	0.00009
	BE-05-07	Fluorite	0.709639	0.00005
	BE-05-14	Fluorite	0.708727	0.00005
	BE-05-20	Fluorite	0.709006	0.00006
	BE-03-04	Fluorite	0.709558	0.00005
	BE-04-23	Fluorite	0.709018	0.00006
	BE-05-02	Fluorite	0.708750	0.00005
	BE-03-32	Fluorite	0.708715	0.00005
	BE-05-22	Fluorite	0.708620	0.00006
	BE-05-25	Fluorite	0.709285	0.00006
	BE-03-26	Calcite	0.708928	0.00005
	BE-03-42	Calcite	0.708564	0.00005
	BE-03-46	Calcite	0.708671	0.00004
	BE-03-52	Calcite	0.708561	0.00005
	BE-05-07	Calcite	0.709000	0.00005
	BE-05-07	Calcite	0.708898	0.00006
	BE-05-21	Calcite	0.709054	0.00005
	BE-05-24	Calcite	0.709659	0.00005
	BE-05-28	Calcite	0.708691	0.00005
	BE-05-04	Dolomite	0.709729	0.00006
	BE-03-17	Barite	0.708522	0.00005
	BE-03-39	Barite	0.708371	0.00005
	BE-03-40	Barite	0.708513	0.00005
	BE-03-52	Barite	0.708516	0.00006
	BE-05-02	Barite	0.708471	0.00005
	BE-05-12	Barite	0.709220	0.00006
La Collada	CO-04-03B	Fluorite	0.710519	0.00006
	CO-04-06B	Fluorite	0.710038	0.00025
	CO-04-03 M	Fluorite	0.710449	0.00005
	CO-04-04 M	Fluorite	0.710438	0.00006
	CO-04-03A	Fluorite	0.710425	0.00006
	CO-04-04A	Fluorite	0.710357	0.00013
	CO-04-06A	Fluorite	0.709448	0.00009
	CO-04-07	Calcite	0.708849	0.00006
	CO-04-13	Calcite	0.708880	0.00013
	CO-04-17	Calcite	0.708947	0.00006
Villabona	VI-04-07	Fluorite	0.708474	0.00005
	VI-04-10	Fluorite	0.708401	0.00005
	VI-04-14	Fluorite	0.708261	0.00006
	VI-04-15	Fluorite	0.708420	0.00005
	VI-04-19A	Fluorite	0.708806	0.00006
	VI-04-19 M	Fluorite	0.708400	0.00005
	VI-07-09	Calcite	0.708359	0.00006
	VI-04-12	Calcite	0.708733	0.00006
	VI-04-14	Calcite	0.708400	0.00005
	VI-05-06	Dolomite	0.708731	0.00005
	VI-04-20	Barite	0.708792	0.00005

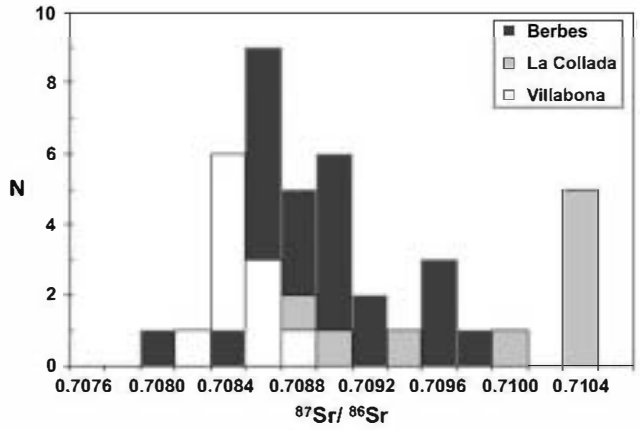

Fig. 6. Histogram of $^{87}Sr/^{86}Sr$ ratios of fluorite, calcite and barite from Berbes, Collada and Villabona districts.

Table 4
Rb–Sr analytical data for trachyandesite rocks from Villaviciosa area (Berbes district).

Sample	Rb (ppm)	Sr (ppm)	Rb/Sr	$^{87}Rb/^{86}Sr$	$^{87}Sr/^{86}Sr$	$^{87}Sr/^{86}Sr$ (abs err)	$^{87}Sr/^{86}Sr$ Initial	εSr
VI-04-18	94.70	183.84	0.515	1.4910	0.711837	0.0005	0.7073[a] 0.7079[b] 0.7085[c]	51.6

[a] Initial $^{87}Sr/^{86}Sr$ ratio recalculated at 213 Ma.
[b] Initial $^{87}Sr/^{86}Sr$ ratio recalculated at 185 Ma.
[c] Initial $^{87}Sr/^{86}Sr$ ratio recalculated at 157 Ma.

5.4.3. Sulphides and barite

Mean $\delta^{34}S$ of pyrite and marcasite from Berbes is $+6.1 \pm 3.3‰$ ($n=7$; 1σ). At La Collada the mean $\delta^{34}S$ of three pyrites is $+9 \pm 0.9‰$ (1σ), with one outlier at $-31.6‰$, and galena at $+5.3‰$. In Villabona, the pyrites give a distinctively lower mean $\delta^{34}S$ of $-12.3 \pm 4‰$ ($n=4$; 1σ) (Tables 7, 8; Fig. 7A,B).

The $\delta^{34}S$ of barite is highly variable, ranging from $+17.2$ to $+30.7‰$ in Berbes (20 samples of BA1) and from $+31.3$ to $+56.7‰$ in Villabona (8 samples of BA2). Most of these $\delta^{34}S$ values are considerably higher than those reported for seawater sulphate between Late Triassic and Late Jurassic (the assumed age range of the deposits), which is $\approx +17‰$ (Claypool et al., 1980). BA2 barite from Villabona displays extraordinarily high $\delta^{34}S$ values, suggesting distinct sulphur source(s) or processes during BA2 formation. The $\delta^{18}O$ of 8 barite samples from Berbes (BA1) range from $+14.7$ to $+17.7‰$, which are close to the assumed values for marine sulphate during Late Triassic to Late Jurassic time span ($\delta^{18}O \approx +13$ to $+15‰$; Claypool et al., 1980). $\delta^{18}O$ values of BA2 barite are higher than those of BA1 ($+15.8$ to $+18‰$; $n=7$). In a $\delta^{34}S$ vs. $\delta^{18}O$ plot (Fig. 8), oxygen and sulphur isotope compositions of BA1 show an apparently positive correlation, with a slope of 0.2. This correlation is not seen in barites from Villabona (BA2).

6. Discussion

6.1. Rare earth element data

Although the ΣREE content of the Asturian fluorites is generally low, fluorites from Villabona have higher concentrations (4.3 to 11.6 ppm) compared to the other two districts (from 0.1 to 2.2 ppm in Berbes and La Collada; see Table 1). PAAS-normalized REE patterns show similar convex-up shape for all the deposits, contrasting with the almost flat REE pattern of the volcanic rocks interbedded with the clastic Permo-Triassic sediments hosting the mineralization.

According to Schwinn and Markl (2005), the total concentration of REE in hydrothermal fluids is controlled by the pH (increasing with

Table 5
Carbon and oxygen isotope data for samples from Villabona, La Collada and Berbes districts.

District	Sample	Mineral	$\delta^{13}C$ (‰ PDB)	$\delta^{18}O$ (‰SMOW)	T_h (°C)	$\delta^{18}O_{fluid}$ (‰SMOW)
Villabona	VI-04-09	Calcite (CC1)	−6.2	20.5	90	2.3
	VI-04-14	Calcite (CC1)	−3.2	21.3	90	3.1
	VI-05-01/1	Calcite (CC1)	−2.5	21.3	90	3.1
	VI-04-12	Calcite (CC2)	−9.3	20.7	90	2.5
	VI-04-15	Calcite (CC2)	−9.7	20.2	90	2.0
	VI-04-17	Calcite (CC2)	−7.8	20.5	90	2.3
	VI-05-01/2	Calcite (CC2)	−2.6	21.4	90	3.2
	VI-05-06	Calcite (CC2)	−14.8	20.0	90	1.8
	VI-05-07	Calcite (CC2)	−5.3	19.4	90	1.2
	VI-05-06/1	Saddle dolomite	−7.9	22.0		
	VI-05-03	Saddle dolomite	−2.2	22.7		
	VI-05-06/2	Saddle dolomite	−5.6	22.6		
La Collada	CO-04-07	Calcite (CC1)	3.6	18.3	120	3.2
	CO−04-13	Calcite (CC1)	3.6	19.9	120	4.8
	CO-04-07/2	Calcite (CC2)	2.8	18.1	120	3.0
Berbes	BE-03-02	Calcite (CC1)	4.6	23.3	130	9.1
	BE-03-09	Calcite (CC1)	2.6	24.1	130	9.9
	BE-03-10	Calcite (CC1)	4.2	20.3	130	6.1
	BE-03-15	Calcite (CC1)	3.6	21.8	130	7.6
	BE-03-26	Calcite (CC1)	6.1	22.7	130	8.4
	BE-03-42	Calcite (CC1)	5.6	20.0	130	5.8
	BE-03-46	Calcite (CC1)	3.7	20.1	130	5.9
	BE-03-52	Calcite (CC1)	3.7	18.3	130	4.1
	BE-05-07	Calcite (CC1)	2.7	17.4	130	3.2
	BE-05-11A	Calcite (CC1)	2.7	17.8	130	3.6
	BE-05-27	Calcite (CC1)	5.2	21.4	130	7.2
	BE-05-28	Calcite (CC1)	5.3	20.7	130	6.5
	BE-03-06	Calcite (CC2)	5.3	22.0	130	7.8
	BE-05-11B	Saddle dolomite	3.2	22.6		
Basement veins	BE-05-24	Calcite (CC1)	1.7	19.7	130	5.5
	BE-05-25	Calcite (CC1)	2.3	21.9	130	7.7
	BE-05-25/2	Calcite (CC1)	0.7	21.6	130	7.4
	BE-05-26	Calcite (CC1)	1.0	21.7	130	7.5
	BE-05-26	Calcite (CC1)	1.4	22.1	130	7.9

$\delta^{18}O_{fluid}$ corresponds to the isotopic composition of water in equilibrium with calcite. Calculations were performed for temperature between 90 and 130 °C using the fractionation equation of O'Neil et al. (1969).

Table 6
Oxygen isotope data for quartz from Berbes and La Collada districts.

District	Sample	Mineral	$\delta^{18}O$ (‰SMOW)	T_h (°C)	$\delta^{18}O_{fluid}$ (‰SMOW)
Berbes	BE-03-31A	Quartz (Q3)	23.0	120	4.6
	BE-03-31B	Quartz (Q3)	23.1	120	4.7
	BE-05-22	Quartz (Q3)	23.5	120	5.0
	BE-03-19	Quartz (Q2)	19.3	120	0.8
	BE-03-21	Quartz (Q2)	20.8	120	2.4
	BE-03-25	Quartz (Q2)	20.5	120	2.0
	BE-05-09	Quartz (Q2)	20.7	120	2.2
	BE-05-19	Quartz (Q2)	22.4	120	4.0
La Collada	CO-04-07	Quartz (Q2)	20.8	120	2.3

$\delta^{18}O_{fluid}$ corresponds to the isotopic composition of water in equilibrium with quartz and barite. Quartz calculations were performed for temperature of 120 °C using the fractionation equation of Clayton et al. (1972).

Table 7
Sulphur isotope data for sulphide minerals from Villabona, Berbes and La Collada districts.

District	Sample	Mineral	$\delta^{34}S$ (‰ V-CDT)
Villabona	VI-05-02	Pyrite	−16.5
	VI-05-Pi1	Pyrite	−10.4
	VI-05-Pi2	Pyrite	−7.6
	VI-04-16	Pyrite	−14.7
Berbes	BE-03-48	Pyrite + marcasite	2.5
	BE 150	Pyrite + marcasite	6.5
	BE-04-15(1)	Pyrite + marcasite	8.8
	BE-04-15(2)	Pyrite + marcasite	8.6
	BE-05-11	Pyrite	0.6
	BE-05-16	Pyrite	7.5
	BE-05-17	Pyrite	8.5
La Collada	CO-04-15	Pyrite	8.3
	CO-04-15(1)	Pyrite	8.9
	CO-04-15(2)	Pyrite	9.9
	CO-04-04	Pyrite	−31.6
	CO-04-04	Galena	5.3

decreasing pH) and the bulk chemical composition of the fluid. As no significant salinity differences between fluids from the three districts have been observed (Sánchez et al., 2006, 2009), the difference in the ΣREE of the fluids could be related to the different types of rocks, leached in the respective areas. Therefore, the lower REE content in fluorites from Berbes could be related to a slightly higher pH of the fluids in that area, facilitated by interaction with carbonates of the basement rocks (Carboniferous). In Villabona where the basement, constituted by Devonian and Carboniferous rocks, is mostly composed by shales and sandstones, fluids would have lower pH carrying higher amounts of REE. Relatively high REE content in some fluorite samples from La Collada can be due to the proximity to the volcanic outcrops (Valverde, 1993) as supported by Sr data (see below).

The general distribution of REE in the analyzed fluorites shows a slight depletion in LREE. According to Bau and Dulski (1995), the fractionation of REE during fluid migration can be due to the sorption of

Table 8
Sulphur and oxygen isotope data for barite from Villabona and Berbes districts.

District	Sample	Mineral	$\delta^{34}S$ (‰ V-CDT)	$\delta^{18}O$ (‰ SMOW)	T_h (°C)	$\delta^{18}O_{fluid}$ (‰ SMOW)
Villabona	VI-05-BA	Barite (BA2)	54.0			
	VI-05-07/1	Barite (BA2)	56.0	16.2	90	0.6
	VI-04-20	Barite (BA2)	44.4	15.8	90	0.3
	VI-05-BA/1	Barite (BA2)	56.7	17.9	90	2.4
	VI-05-BA/2	Barite (BA2)	55.8	17.2	90	1.7
	VI-05-08	Barite (BA2)	55.3	17.8	90	2.3
	VI-05-09	Barite (BA2)	32.1	18.0	90	2.5
	VI-05-05	Barite (BA2)	31.3	16.6	90	1.12
Berbes	BE-03-14	Barite (BA1)	20.1			
	BE-03-17	Barite (BA1)	23.8	14.8	140	4.5
	BE-03-18	Barite (BA1)	20.2			
	BE-03-24	Barite (BA1)	26.1	15.7	140	5.3
	BE-03-34	Barite (BA1)	19.6			
	BE-03-35	Barite (BA1)	19.2			
	BE-03-39	Barite (BA1)	21.0	14.8	140	4.4
	BE-03-40	Barite (BA1)	21.9	15.2	140	4.9
	BE-03-47	Barite (BA1)	18.1			
	BE-05-02	Barite (BA1)	23.0	14.7	140	4.4
	BE-05-12	Barite (BA1)	28.1	16.3	140	6.0
	BE-05-14	Barite (BA1)	30.7	17.7	140	7.4
	BE-05-15/1	Barite (BA1)	24.0			
	BE-05-15/2	Barite (BA1)	24.3			
	BE-05-18	Barite (BA1)	25.8			
	BE-05-21	Barite (BA1)	17.2	14.7	140	4.4
	BE-05-24	Barite (BA1)	27.6			
	BE-05-25/1	Barite (BA1)	26.9			
	BE-05-25/2	Barite (BA1)	27.1			
	BE-05-BA	Barite (BA1)	28.2			

Barite calculations were performed for temperature of 90 °C in Villabona and 140 °C in Berbes using fractionation equation of Kusakabe and Robinson (1977).

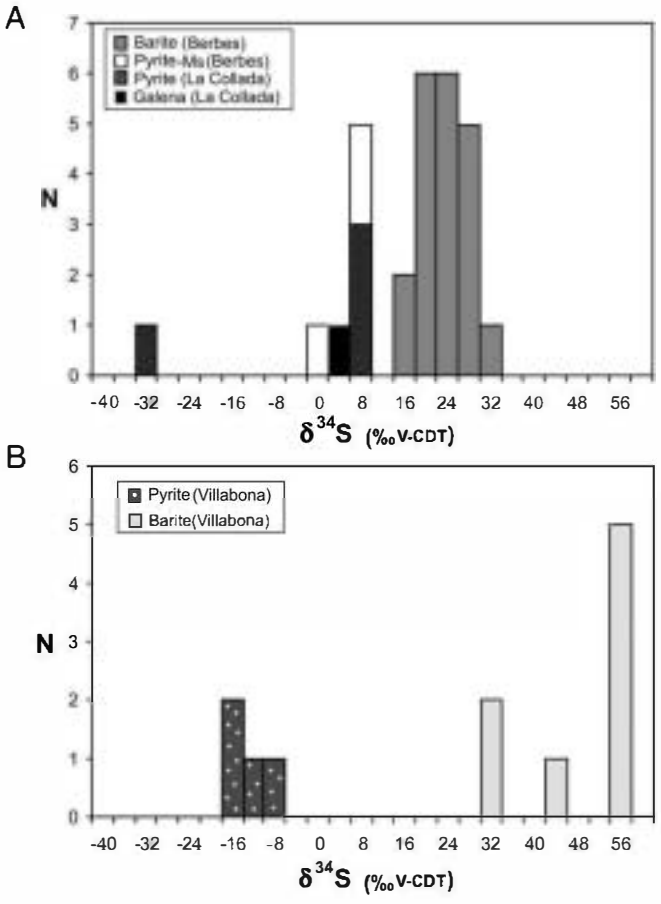

Fig. 7. $\delta^{34}S$ histogram for sulphates (barite) and sulphides (pyrite, marcasite and galena): (A) Berbes and La Collada deposits. (B) Villabona deposit.

REE on mineral surfaces or to REE complexation in solution. During fluid migration, when sorption prevails, LREE-enriched patterns are produced whereas if REE-complexation dominates, LREE-depleted patterns would result as HREE are more effectively complexed with fluoride ions than LREE (Wood, 1990a,b; Haas et al., 1995). La/Lu ratios, a measure of REE fractionation, are <1 decreasing from Berbes to Villabona and suggesting a stronger complexation of HREE in ligand-rich solutions (Bau, 1991). As the chemical complexation is compatible with the presence of Ca-rich brines in the deposits, complexation of HREE during migration of the mineralizing fluids seems to be a plausible explanation for the REE distribution patterns. Moreover, HREE complexation could have been more important in Villabona, where, according to Sánchez et al. (2009), fluids reached the depositional site after flowing through a longer path compared to Berbes.

However, the variation in LREE could also be explained by a mixing process involving a REE-depleted hydrothermal fluid and a LREE-enriched fluid with a signature similar to that of most crustal rocks. Thus, the hydrothermal system in Villabona would be dominated by a REE-enriched fluid after interaction with clastic rocks (probably the

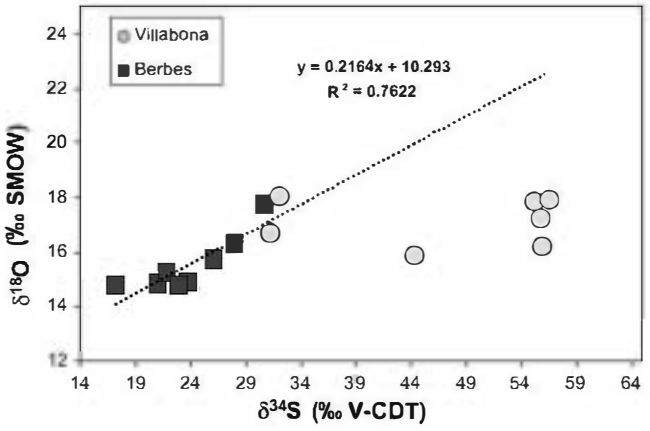

Fig. 8. $\delta^{34}S$ *vs.* $\delta^{18}O$ diagram for barites from Berbes and Villabona districts.

Devonian and Carboniferous basement) whereas in Berbes and La Collada the dominating fluid would be REE-poor, after interaction with carbonates. A fluid mixing model is supported by fluid inclusion (Sánchez et al., 2009), stable and radiogenic isotope data (see below).

The REE differences of fluorite from Villabona and Berbes and La Collada raise the question of whether the REE patterns, the Ce and Eu anomalies may be used to trace the source of REE. A general feature of REE in the studied fluorites is the lack of significant Eu anomalies (either positive or negative) and the presence of a positive Ce anomaly in Berbes. The lack of positive Eu anomalies has been related to temperatures of hydrothermal fluids lower than 250 °C (Bau and Möller, 1992), consistent with the fluid inclusion data which indicate temperatures of formation lower than 170 °C (Sánchez et al., 2009). Although fluorite has co-precipitated with sulphides (pyrite inclusions are typically found in fluorite) indicating reducing conditions, in low-temperature acidic fluids, Eu^{3+} can be stable with reduced sulphur (Bau, 1991).

The positive Ce anomaly in samples from Berbes, might be explained through two processes: (1) reduction of Ce(IV) to Ce(III) at the depositional site, increasing the Ce content of the fluid available to be incorporated into fluorite; and (2) the Ce content of the fluids was already Ce(III)-enriched before fluorite precipitation (inherited anomaly). In any case, the positive Ce anomaly of Berbes fluorite suggests that environment during fluorite formation was reducing with respect to the Ce(IV)/Ce(III) redox system.

Marine carbonates show negative Ce anomalies and commonly have low REE concentrations. Ce in igneous rocks and clastic sediments is generally Ce(III). REE concentration in aluminosilicate rocks is usually several orders of magnitude higher that of marine limestones (Parekh et al., 1977). Then, as stated before, the difference in the REE content between Villabona and Berbes–La Collada could be due to fluids that interacted with different lithologies, clastic rocks and carbonates respectively. However, fluorite from Berbes reflects a positive Ce anomaly, contrary to what would be expected if carbonates were the main source of REE in the fluids, unless other processes increasing the Ce(III) concentration operated during fluorite deposition. The higher temperatures of hydrothermal fluids coupled with a more reducing conditions (presence of bitumen and hydrocarbon-bearing inclusions in fluorite) during fluorite deposition in Berbes could have increased of the Ce(III) content in the fluids. According to Bau et al. (1997), formation and subsequent removal of Mn- and/or Fe-oxyhydroxides from seawater leads to decreasing LREE/HREE ratios, and increasing the negative Ce anomaly in seawater. However, the dissolution of these particles below the redox-boundary generates higher LREE/HREE ratios, and smaller negative or even positive Ce anomaly in anoxic conditions.

The Tb/Ca and Tb/La ratios have been used to discriminate fluorite occurrences according to their sedimentary, hydrothermal and pegmatitic affinities (Möller et al., 1976) although the interpretation of such diagrams has been questioned (Gagnon et al., 2003). In Tb/Ca *vs* Tb/La plots, Möller et al. (1976) interpreted crystallization and remobilization trends as resulting from progressive incorporation of REE into fluorite during hydrothermal precipitation. We have examined the composition of fluorite analyzed in this study in terms of the fields and trends defined by Möller et al. (1976), using a constant, stoichiometric abundance of Ca in ideal fluorite. In the Tb/Ca *vs*. Tb/La diagram (Fig. 9), fluorite samples plot within the sedimentary field, like most MVT deposits, suggesting dissolution and incorporation of calcium-rich carbonate rocks by the ore-forming solutions (Möller et al., 1976).

6.2. Sm–Nd data and the age of the Villabona

The Sm–Nd correlation diagram shows the isotopic data for the fluorite from Villabona (Fig. 5), which yield an isochron corresponding to an age of 185±28 Ma (Late Triassic to Late Jurassic). This age

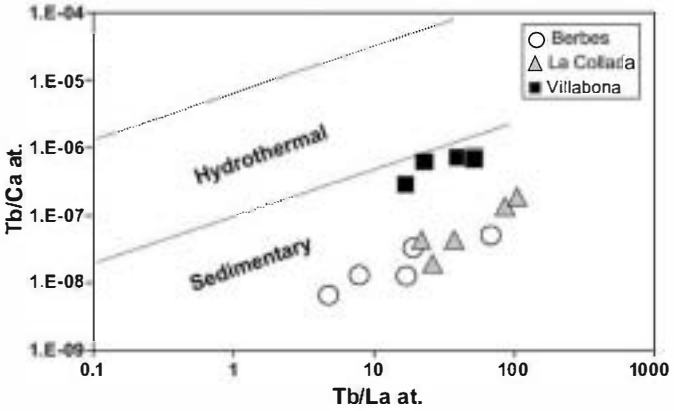

Fig. 9. Logarithmic plot of Tb/Ca *vs.* Tb/La in fluorite from Berbes, La Collada and Villabona.

overlaps previously calculated Sm–Nd ages in fluorites from the Iberian Peninsula: the barite–fluorite (Pb–Zn) veins of the Sierra del Guadarrama yielded an age of 145 ± 18 Ma (Galindo et al., 1994) and the Rigrós fluorite–barite vein of the Catalonian Coastal Ranges an age of 136 ± 32 Ma (Piqué et al., 2008). Similar ages have been reported for some fluorite deposits in France (i.e. Chaillac, Massif Central; Sizaret et al., 2004) and for other mineralizations in the Schwarzwald region, SW Germany (Pfaff et al., 2009). In the Asturian fluorspar district, fluid movement and mineralization may be related to early pre-rift thermal events during the Early Jurassic. As no igneous activity has been reported in the area since the Permian, an igneous origin for the fluids is unlikely. In contrast, the narrow range of the initial Nd (εNd) isotopic composition of fluorite samples from Villabona, −9.8 to −9.3 is consistent with mineralizing fluids equilibrated with sedimentary rocks. Bau et al. (2003) report εNd values for Carboniferous limestones in the Pennine Orefield (England) between −8.9 and −9.4, very close to the values of Villabona fluorites.

6.3. Sr isotope data

The $^{87}Sr/^{86}Sr$ ratios in fluorite likely reflect the original values in the solution during precipitation considering that the Rb/Sr ratios are low (<0.06). The widespread variation in the $^{87}Sr/^{86}Sr$ ratios, from 0.7080 to 0.7105, suggests the existence of more than one source of Sr. Two possible candidates can be considered as the end-member solutions: a non-radiogenic source, either seawater of Upper Triassic–Upper Jurassic age ($^{87}Sr/^{86}Sr \approx 0.7070$; Burke et al., 1982), or waters that interacted with limestones, either Triassic, Jurassic or Carboniferous ($^{87}Sr/^{86}Sr \approx 0.7080$; Koepnick et al., 1990) and a more radiogenic source having $^{87}Sr/^{86}Sr$ ratios>0.7105, probably related to fluids that interacted with rocks containing more radiogenic minerals (aluminosilicate-dominated rocks), which are present in the basement as well as in the Permo-Triassic cover.

Permo-Triassic trachyandesites, considered as a potential source for fluorine (García Iglesias and Loredo, 1994), could also be a source of Sr. Leaching of these rocks could contribute to the hydrothermal fluids with $^{87}Sr/^{86}Sr$ values similar to the other potential Sr sources. Unfortunately, the calculated $^{87}Sr/^{86}Sr$ ratio of trachyandesites at 185 Ma (0.70791; Table 4), does not allow the unique distinction of these rocks as source of either Sr or F.

Notwithstanding, the $^{87}Sr/^{86}Sr$ ratios of fluorite in the three districts can be explained assuming different mixing proportions between the "end-member" solutions. During fluorite precipitation the more radiogenic source would be the dominant in La Collada (mean $^{87}Sr/^{86}Sr$ of fluorite: 0.71024; $n=7$), whereas in Villabona the contribution of the less radiogenic fluid would be more important (mean $^{87}Sr/^{86}Sr$ of fluorite: 0.70846; $n=6$). These higher values in La Collada can be due to the proximity of the volcanic outcrops

(trachyandesites) instead of the basement rocks as in Berbes and Villabona districts. As the Carboniferous basement in Villabona is mainly siliciclastic, the low radiogenic source fluids must be either Triassic–Jurassic seawater or any other type of fluid equilibrated with limestones of these ages.

According to the mineral paragenesis, calcite and barite in the three studied deposits precipitated later than fluorite. In Berbes and Villabona, the $^{87}Sr/^{86}Sr$ of both minerals is similar to that of fluorite, suggesting that the precipitating conditions in these areas did not significantly change during the different stages of mineralization. However, in La Collada, calcite has lower $^{87}Sr/^{86}Sr$ ratios (mean $^{87}Sr/^{86}Sr = 0.70889$; $n = 3$) than fluorite, suggesting that the late stages of mineralization were dominated by a less radiogenic fluid. Therefore, even though the individual sources of Sr cannot be uniquely identified, Sr isotope data reinforce the idea of mixing as a main cause of fluorite deposition as supported by fluid inclusion, REE and stable isotope data (see below).

6.4. Carbonate data

As T_h in calcites from the three deposits are slightly different (Sánchez et al., 2009), the following modal values have been taken for the calculation of the $\delta^{18}O$ of the fluid in equilibrium with precipitating carbonates: 130 °C for Berbes, 120 °C for La Collada and 90 °C for Villabona (see Table 5). Using the equation of O'Neil et al. (1969) for the equilibrium between calcite and water, the calculated $\delta^{18}O$ of the fluid in isotopic equilibrium during calcite precipitation (CC1 and CC2) varies between +3.0 and +9.9‰ in Berbes and La Collada and from +1.2 and +3.2‰ in Villabona.

The more negative $\delta^{13}C$ values of calcites from Villabona (between −14.8 and −2.2‰) compared to those of Berbes and La Collada indicate a contribution of organic-derived carbon during precipitation. In Villabona area, situated 4 km to the south of Moscona mine, the underlying Carboniferous sequence (Stephanian) contains coal seams and therefore, the presence of an isotopically lighter carbon source could be related to the interaction of the fluids with coal-bearing strata.

The $\delta^{13}C$–$\delta^{18}O$ plot (Fig. 10) is especially useful to obtain information on temperature and fluid composition. Two different $\delta^{13}C$–$\delta^{18}O$ trends are distinguished: the first corresponds to carbonates from La Collada and Berbes, showing a wide range in $\delta^{18}O$ and small $\delta^{13}C$ variation, and the second, corresponding to calcites from Villabona, with a narrower $\delta^{18}O$ and a wider $\delta^{13}C$ range.

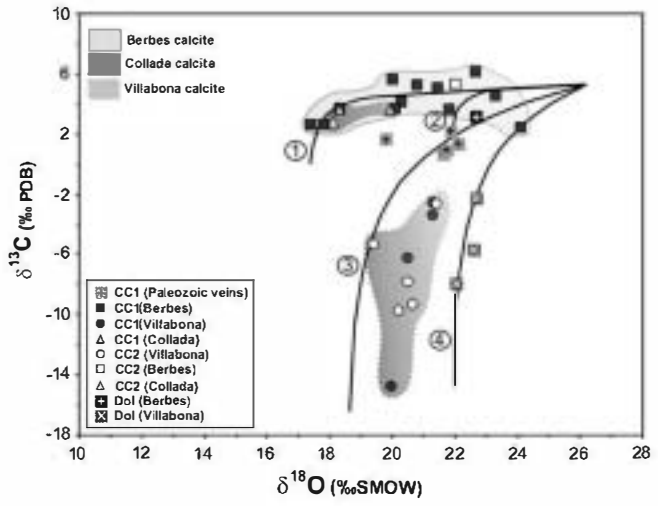

Fig. 10. $\delta^{13}C$–$\delta^{18}O$ diagram for calcites and dolomites from Asturias deposits. Isotopic composition for calcite and dolomite precipitated by fluid mixing. Lines are showing temperature interval for carbonated precipitation. Line (1): $T_{brine} = 260$ °C, $T_{surficial}$ (Berbes) = 60 °C; Line (2): $T_{brine} = 170$ °C, $T_{surficial}$ (Berbes) = 60 °C; Line (3): $T_{brine} = 230$ °C, $T_{surficial}$ (Villabona) = 60 °C; Line (4): $T_{brine} = 170$ °C, $T_{surficial}$ (Villabona) = 60 °C.

The $\delta^{13}C$–$\delta^{18}O$ trend of hydrothermal calcites (CC1 and CC2) can be explained from a mixing between a brine having a $\delta^{13}C$ of +2‰ in Berbes and −15‰ in Villabona, a $\delta^{18}O = +10$‰, at temperatures of 260 to 170 °C in Berbes and of 230 to 170 °C in Villabona, with a fluid of surficial origin with $\delta^{13}C = +4$‰; $\delta^{18}O = +3$‰ at a temperature of 60 °C. The calculations were performed assuming H_2CO_3 as the dominant carbon species in the saline brine and $(HCO_3)^-$ in the low-temperature fluid and a total carbon concentration ratio (brine/meteoric water) of 0.5. Both C and O-isotope trends are satisfactorily reproduced within the boundaries of the mixing models (Fig. 10) which suggest that mixing was the dominant process in the formation of hydrothermal carbonate. It is interesting to observe that carbon and strontium isotope compositions and REE content of the brine were not homogeneous, and that local control by the presence of particularly organic matter-rich rocks can exert a strong influence as in the Villabona area.

According to Sánchez et al. (2009), on the basis of halogen data of fluid inclusions, the brine has acquired its salinity by halite dissolution present in sediments of Triassic and Jurassic age and interaction with basement rocks. The temperature of fluorite and calcite precipitation was around 130 °C in Berbes and 90 °C in Villabona, but as homogenization temperatures are the result of mixing at the depositional sites, the temperature of the brine prior to mixing was probably higher. Therefore, a temperature range between 260 and 170 °C for the brine has been chosen in the Berbes area and between 230 and 170 °C in Villabona, where the homogenization temperatures are lower.

As during the interaction with carbonate rocks, the isotopic composition of fluids is shifted to higher $\delta^{18}O$ values (Schwinn et al., 2006), a $\delta^{18}O = +10$‰ for the deep brine has been assumed. For carbon, a $\delta^{13}C = +2$‰ has been taken in Berbes considering that the brines isotopically exchanged with carbonates in the Carboniferous basement. In Villabona, the mixing model was calculated assuming that the basinal brine shifted the carbon isotope composition to a $\delta^{13}C \approx -15$‰ after interacting with a light carbon source (Stephanian coal seams).

As a surficial fluid end member, modified rainwater infiltrating the Mesozoic cover has been considered. Surface waters can reach $\delta^{13}C$ of +4‰ after flowing through limestones, which are abundant in both, Jurassic and Triassic age series. The $\delta^{18}O$ values may be highly variable but considering that these waters probably dissolved carbonates, a value of +3‰ has been assumed. A temperature of 60 °C for the surficial fluid has been taken assuming a thermal gradient of 40 °C/km (compatible with by the intense tectonic activity during Upper Triassic to Upper Jurassic times in the area) and an infiltration of waters to depths of less than 1 km (the maximum depth of the Mesozoic cover).

Due to the small size, no homogenization temperatures could be obtained from fluid inclusions in saddle dolomite and therefore the isotopic composition of the fluid could not be calculated. However, as dolomite precipitated later than calcite and assuming that the hydrothermal system evolved to lower temperatures, the higher $\delta^{18}O$ values of dolomite (+22 to +22.7‰) could be explained by a low-temperature isotopic exchange of dolomite with meteoric waters during the late stages of the mineralization. The carbon isotope composition of saddle dolomite is buffered by the respective carbonate precursors, i.e. they have similar $\delta^{13}C$ values to those of associated calcites in both deposits.

6.5. Quartz data

Assuming a temperature of formation for Q2 of 120 °C, deduced from microthermometry of fluid inclusions (Sánchez et al., 2009), the calculated $\delta^{18}O$ of the fluid (using the equation of Clayton et al., 1972)

varied from +0.8 to +4.0‰ (Table 6), values slightly lower than those calculated during calcite formation but consistent with mixing between basinal brines and surficial waters or with a change in the $\delta^{18}O$ of the fluid over time. Microthermometric data from hydrocarbon-bearing fluid inclusions in Q3 (only found in Berbes) indicate similar temperatures of formation (120 °C; Arcos and Tornos, 1997). The calculated $\delta^{18}O$ of the fluids in isotopic equilibrium with quartz (Q3) ranged from +4.6 to +5.0‰, values that are higher compared to fluids involved in the precipitation of Q2 and pointing to a change in the origin or in the mixing proportions of fluids during late stages of mineralization. The abundance of hydrocarbons trapped in late quartz from Berbes (Q3) might be related to the distillation of organic matter during the interaction with hot, basinal-derived fluids, producing a solid residue (pyrobitumen) and a liquid phase (hydrocarbons), some of which could be trapped in fluorite but especially in late quartz (Q3) after mobilization.

6.6. S isotope data

A striking feature of the Asturian fluorite deposits is the large difference in the $\delta^{34}S$ values of sulphides (see Table 7; Fig. 7A,B) and in the $\delta^{34}S$ and $\delta^{18}O$ of sulphates between Villabona and Berbes–La Collada areas (see Table 8).

In Villabona (Fig. 7B), the high $\delta^{34}S$ values of barite (up to +56.7‰) and low $\delta^{34}S$ values of sulphides (down to −16.5‰) are compatible with the large isotopic fractionation values during bacteriogenic sulphate reduction processes (BSR) in a closed system with respect to sulphate. BA2 is a later generation of barite only recognized in Villabona (Fig. 3). Bacterial reduction primarily occurs at temperatures lower than 80 °C (Machel, 2001), although in some hydrothermal vent sites, bacterial reduction has been found to occur up to 110 °C (Jørgensen et al., 1992). Unfortunately, no microthermometric data from BA2 at Villabona are available, as fluid inclusions show clear evidences of leaking. However, homogenization temperatures of fluid inclusions in fluorite and CC1 (precipitated before BA2) are around 90 °C, clearly lower than those found in Berbes and La Collada. Therefore, if this was the highest temperature reached in Villabona, bacteriogenic activity could have been present at the depositional site. We can thus envisage a scenario where sulphate, dissolved in a fluid of surficial origin trapped within the sediments, was being bacteriogenically reduced in the presence of organic matter in a closed system.

Similar high $\delta^{34}S$ values were reported by Richardson et al. (1988) in late stage barite from the Illinois–Kentucky district, U.S.A., and were explained by a combination of inorganic and bacterially catalyzed reduction processes involving thiosulphate in the presence of organic matter (Spirakis, 1991). This hypothesis cannot be discarded as the presence of organic matter associated with fluorite and sulphides (hydrocarbon-bearing fluid inclusions and bitumen) is a common feature in the studied deposits.

Compared to $\delta^{34}S$, $\delta^{18}O$ values of barites from Villabona (+15.8 to +18.0‰) are much less variable and no clear correlation seems to exist between $\delta^{34}S$ and $\delta^{18}O$. BSR processes typically produce $\delta^{34}S$–$\delta^{18}O$ linear correlations with slopes of 4 (Mizutani and Rafter, 1969; Claypool et al., 1980), although other studies report slopes between 0.3 and 3, resulting from the isotopic effects of chemical reactions in the oxidative portion of the diagenetic sulphur cycle (Canfield and Thamdrup, 1994; Habitcht and Canfield, 1997; Böttcher et al., 2001). The lack of a correlation between $\delta^{34}S$ and $\delta^{18}O$ in Villabona might be related to chemical reactions involving sulphur species with intermediate oxidation states.

Barite from Berbes (BA1), paragenetically early with respect to barite from Villabona (BA2), has distinctive, lower and more homogeneous $\delta^{34}S$ values (from +17.2 to +30.7‰). The positive $\delta^{34}S$ values (Table 7, Fig. 7A) of most sulphides from Berbes and La Collada (from +0.6 to +9.9‰, except sample CO-04-04: −31.6‰) are also consistent with sulphate reduction processes. $\delta^{34}S$ and $\delta^{18}O$ values show a linear correlation with a slope of 0.2 (Fig. 8), close to the values reported in BSR processes. However, homogenization temperatures of fluid inclusions indicate that at Berbes, barite (BA1) formed between 140 and 150 °C (Cardellach et al., 2007), exceeding the conditions capable of sustaining efficient bacterial processes (>120 °C). Thus, biogenic reduction, if present, should have occurred away from the ore zone and/or prior to the mineralizing event.

Alternatively, at Berbes, sulphate reduction could have been thermochemically driven (TSR) when hot ascending brines mixed with organic matter and sulphate-rich fluids present at the depositional site. However, although the sulphur isotope fractionation between sulphides and sulphates at Berbes are within the 10 to 20‰ range reported by Kiyosu and Krouse (1990) as typical for kinetically controlled fractionations during TSR processes between 100 and 200 °C, a TSR process would not explain the linear correlation between the $\delta^{34}S$ and $\delta^{18}O$ of barite. Therefore, in Berbes, BSR prior to mixing with the hot brine also seems to be a plausible mechanism of sulphate reduction. The lower $\delta^{34}S$ values of barite from Berbes (from +17.2 to +30.7‰) compared to Villabona (+31.3 to +56.7‰) could be due to differences in some of the parameters controlling the kinetics of the reduction process, although closed system effects, with respect to the sulphate reservoir, are clearly seen here too.

Sulphate-bearing waters of surficial origin were probably trapped in organic matter-bearing, porous sedimentary rocks (piedmont breccias, carbonates, sandstones…) of the Permo-Triassic cover. The sulphate source of these waters could either be related to seawater or to the dissolution of evaporites of Upper Triassic to Upper Jurassic age ($\delta^{34}S \approx +13$ to +17‰; Claypool et al., 1980), a hypothesis compatible with Sr isotope data (see above). The main source of reduced sulphur for sulphide precipitation was thus related to the reduction of sulphate, although a small contribution of H_2S from the basinal brines cannot be discounted. Sulphides precipitated when metal-carrying brines encountered the H_2S in the Permo-Triassic reservoirs.

It is interesting to point out that in Villabona the mixing occurred within carbonates overlying marls–limestones of Permo-Triassic age, whereas in Berbes the surficial fluids were hosted in piedmont breccias situated at the bottom of the Permo-Triassic section, that are related to the erosion of the Paleozoic basement. These different lithologies point to a shallower origin for the fluorite deposits in Villabona, favouring cooler temperatures and BSR reduction.

The variability of fluid sources in the studied deposits can also be recognized during barite precipitation. Assuming isotopic equilibrium between sulphate and water and a $T = 140$ °C, the $\delta^{18}O$ of the fluid during barite precipitation at Berbes (BA1) would range between +4.4 and +7.4‰ (Table 8), suggesting the presence of basinal fluids. In contrast, in Villabona, the calculated $\delta^{18}O$ values range from +0.3 to +2.5‰ (assuming a deposition temperature of 90 °C, similar to that obtained in fluorite), pointing to a system dominated by fluids of surficial origin. As mixing between sulphate-rich and Ba-bearing solutions is the most common process for barite precipitation, the higher $\delta^{18}O$ of barite in Berbes (BA1) could reflect mixing dominated by the isotopically heavier component (basinal fluid) whereas in Villabona the late stage barite (BA2) could result from a mixing dominated by the ^{16}O-enriched component (surficial fluid). Therefore, different proportions of the end members during mixing could be a possible explanation for the regional-scale differences in the fluid chemistry of the fluids involved in the formation of the Asturian fluorite deposits.

The amount of sulphides and sulphates (barite) in the Asturian fluorite deposits is small in spite of the presence of high concentration of dissolved metals (Pb, Zn, Cu etc.) in the hydrothermal fluids (Sánchez et al., 2009). Therefore, the limiting factor for the presence of sulphides was probably the availability of reduced sulphur. The amount of H_2S generated by sulphate reduction processes (either TSR or BSR) depends on the amount and availability of sulphate and

organic matter. Therefore, as organic matter is present in all the studied deposits the availability of sulphate was probably the limiting factor affecting the amount of precipitated barite and sulphides, and it is therefore not surprising that sulphate $\delta^{34}S$ shows marked closed system behaviour.

7. Conclusions

The Asturian fluorspar deposits preferentially occur in the margins of a Mesozoic basin, which overlies the basement of Paleozoic and Precambrian age. Although the geological framework is similar and fluorite dominates in all deposits, our study shows that across this area — of less than 50 km — an astonishing variability of sources and processes has led to each area having its own distinctive characteristics. Although variations in homogenization temperatures of fluid inclusions were already reported by García Iglesias and Loredo (1994) and Sánchez et al. (2009), important variations in the REE content as well as in the stable and radiogenic isotopes of gangue and ore minerals have been observed.

The two mineralized areas, Berbes–La Collada and Villabona, differ in host rock and position within the Mesozoic basin. The Berbes and La Collada deposits are situated close to the depocenter of the basin and are hosted by piedmont breccias at the bottom of the Permo-Triassic section. Volcanic rocks (trachyandesites) interbedded within the Permo-Triassic sediments outcrop near these deposits. Villabona is situated on the western margin of the basin and is hosted by silicified carbonate rocks of Permo-Triassic age. This, together with the presence of different basement rocks in the Villabona area (siliciclastics with coal seams) with respect to Berbes–La Collada (carbonates), influenced the chemistry of the brine, providing particular, distinct geochemical signatures in each district.

The ΣREE content of fluorite increases from Berbes to Villabona by an order of magnitude. This increase may be related to the pH of the fluids, which in turn is controlled by the basement rocks: limestones in La Collada and Berbes, buffering the fluid to alkaline pHs, and mainly aluminosilicate rocks in Villabona, buffering the fluid to more acidic pHs. The roof shaped REE pattern of fluorites contrasts with the flat pattern of the volcanics interbedded within the sedimentary rocks of Permo-Triassic age. The positive Ce anomaly, only present in fluorites from Berbes, suggests a reducing environment of deposition with respect to the Ce(IV)/Ce(III) pair. The presence of tiny inclusions of sulphides (pyrite and chalcopyrite) within fluorite crystals is consistent with this hypothesis.

The La/Lu ratio in fluorites decreases from a mean value of 0.36 in Berbes, 0.17 in La Collada to 0.09 in Villabona pointing to a strong fractionation between LREE and HREE, especially in Villabona. This difference suggests that either: 1) the hydrothermal fluids leached different rocks in each area, 2) the longer pathway from the assumed recharge area (close to La Collada; Sánchez et al., 2009) to Villabona involved a higher HREE complexation during migration, or 3) a mixing occurred between a REE-depleted and a REE-enriched fluids, the latter prevailing in Villabona and the former in Berbes and La Collada. However, these three effects may have occurred simultaneously.

Sr isotope composition of fluorite is characterized by a variable range of $^{87}Sr/^{86}Sr$ ratios in Berbes (0.7080 to 0.7096) and La Collada (0.7094 to 0.7105), compared to Villabona (0.7083 to 0.7088). These widespread ratios are interpreted as the result of mixing in different proportions of a low radiogenic source ($^{87}Sr/^{86}Sr$ ratios<0.7080), compatible with seawater or limestones of Triassic–Jurassic age, and a more radiogenic source (>0.7105), reflecting the aluminosilicate-rich rocks present in the Triassic cover and in the Paleozoic basement. The more radiogenic end member would predominate in Berbes and La Collada, whereas the lower $^{87}Sr/^{86}Sr$ values in Villabona suggest the predominance of the less radiogenic end member. Calcite and barite show values within the reported range for fluorites, indicating that the Sr sources were similar during the formation of fluorite and gangue minerals. The Permo-Triassic trachyandesitic lavas were suggested to be a source of fluorine by García Iglesias and Loredo (1994) but unfortunately, this hypothesis could not be confirmed from our REE and Sr isotope data and thus, the origin of fluorine remains an open question.

The $\delta^{13}C$–$\delta^{18}O$ trend of hydrothermal calcites (CC1 and CC2) suggests that mixing was also the dominant process in the formation of hydrothermal carbonates. The distribution of carbon and oxygen isotope data can be modelled through a mixing between a brine having a $\delta^{13}C$ of +2‰ in Berbes and −15‰ in Villabona, a $\delta^{18}O = +10‰$, at temperatures of 260 to 170 °C in Berbes and of 230 to 170 °C in Villabona, with a fluid of surficial origin with $\delta^{13}C = +4‰$; $\delta^{18}O = +3‰$ at a temperature of 60 °C. The carbon isotope composition of the brine was not homogeneous, and a local control by the presence of particularly organic matter-rich rocks (coal seams) exerted a strong influence in the Villabona area.

The range of $\delta^{34}S$ values of barite (from +17.2 to +30.7‰ in BA1 and from +31.3 to +56.7‰ in BA2) and the correlation between $\delta^{34}S$ and $\delta^{18}O$ in Berbes, are explained from the contribution of different sulphate reduction processes (BSR and TSR) affecting surficial fluids trapped in the sedimentary rocks of the Permo-Triassic cover. In Villabona, the $\delta^{34}S$ values of sulphide could only have been produced by sulphate reduction processes (BSR) in an open system, while $\delta^{34}S$ values of barite are compatible with a BSR in a closed system. The sulphate source could either be related to seawater or to dissolution of evaporites of Jurassic age ($\delta^{34}S \approx +17$ to +20‰; Claypool et al., 1980) a hypothesis compatible with Sr isotope data. Reduction of sulphate produced H_2S which would accumulate at the depositional site. Sulphides and barite precipitated when metal-carrying basinal brines mixed with sulphate and H_2S-bearing reservoirs although a small contribution of H_2S from the basinal brines cannot be discarded. The calculated $\delta^{18}O$ of fluids in equilibrium with barite in Berbes (+4.4 to +7.4‰) suggests the predominance of the basinal brine during barite precipitation whereas the values obtained in late barite from Villabona (+0.3 to +2.5‰) point to the prevalence of a fluid of surficial origin. Sulphur content is limited in all deposits supporting the closed system behaviour noted in sulphate data, especially in Villabona.

The Sm–Nd age of fluorite from Villabona is 185 ± 28 Ma, placing its formation between Late Triassic and Late Jurassic. Therefore, fluid movement and mineralization in the Asturian fluorspar district seem to be related to pre-rift or rift thermal events prior or contemporaneous to the Atlantic Ocean opening. The geochemical features and ages of the Asturian fluorites are similar to other fluorite-rich districts in the Iberian Peninsula and Western Europe, which are associated to hydrothermal activity related to the rifting stages that took place from Early Jurassic to Upper Cretaceous times.

Acknowledgments

This research has been funded through the research project BTE2003-01346, Ministerio de Educación y Ciencia. We are in debt to MINERSA for providing the access to the mines. We gratefully acknowledge the contribution of Dr. J. Marín for the field assistance and helpful discussions. SUERC is funded by NERC and the consortium of Scottish Universities. AJB is funded by NERC support of the Isotope Community Support Facility at SUERC. H.A. Gilg and an anonymous reviewer are also thanked for their critical reviews, which helped improve the manuscript.

References

Arcos, D., Tornos, F., 1997. Hydrocarbon fluid inclusions in quartz crystal from the fluorite stratabound deposits of Berbes (Spain). XIV ECROFI, Nancy, France, pp. 10–16.

Bau, M., 1991. Rare-earth element mobility during hydrothermal and metamorphic fluid–rock interaction and the significance of the oxidation state of europium. Chemical Geology 93, 219–230.

Bau, M., Dulski, P., 1995. Comparative study of yttrium and rare earth element behaviour in fluorine-rich hydrothermal fluids. Contributions to Mineralogy and Petrology 119, 213–223.

Bau, M., Möller, P., 1992. Rare earth element fractionation in metamorphogenic hydrothermal calcite, magnesite and siderite. Mineralogy and Petrology 45, 231–256.

Bau, M., Möller, P., Dulski, P., 1997. Yttrium and lanthanidhes in eastern Mediterranean seawater and their fractionation during redox-cycling. Marine Chemistry 56, 123–131.

Bau, M., Romer, R.L., Lüders, V., 2003. Tracing element sources of hydrothermal mineral deposits: REE and Y distribution and S–Nd–Pb isotopes in fluorite from MVT deposits in the Pennine Orefield, England. Mineralium Deposita 38, 992–1008.

Behr, H.J., Gerler, J., 1987. Inclusions of sedimentary brines in post-Variscan mineralizations in the Federal Republic of Germany — a study by neutron activation analysis. Chemical Geology 61, 65–77.

Behr, H.J., Horn, E.E., Frenzel-Beyme, K., Reutel, C., 1987. Fluid inclusions characteristics of the Variscan and post-Variscan mineralizing fluids in the Federal Republic of Germany. Chemical Geology 61, 273–285.

Böttcher, M.E., Thamdrup, B., Vennemann, T.W., 2001. Oxygen and sulfur isotope fractionation during anaerobic bacterial disproportionation of elemental sulfur. Geochimica et Cosmochimica Acta 65, 1601–1609.

Burke, W.H., Denison, R.E., Hetherington, E.A., Koepnick, R.B., Nelson, H.F., Otto, J.B., 1982. Variations of seawater $^{87}Sr/^{86}Sr$ throughout Phanerozoic time. Geology 10, 516–519.

Canals, A., Cardellach, E., 1993. Strontium and sulphur isotope geochemistry of low temperature barite–fluorite veins of the Catalonian Coastal Range (NE Spain): a fluid mixing model and age constraints. Chemical Geology 104, 269–280.

Canfield, D.E., Thamdrup, B., 1994. The production of ^{34}S-depleted sulfide during bacterial disproportionation of elemental sulphur. Science 266, 1973–1975.

Cann, J.R., Banks, D.A., 2001. Constraints on the genesis of the mineralization of the Alston Block, Northern Pennine Orefield, northern England. Proceedings of the Yorkshire Geology Society 53, 187–196.

Cardellach, E., Corbella, M., Sánchez, V., Vindel, E., Boyce, A.J., et al., 2007. Origins of Fluids Associated to Gangue Minerals in Fluorite Deposits of Asturias (N Spain). In: Andrew, C.J. (Ed.), Digging Deeper: Proceedings of the Ninth Biennial SGA Meeting, Dublin, vol. 2, pp. 1311–1314.

Chesley, T.J., Halliday, A.N., Kesler, T.K., Spry, P.G., 1994. Direct dating of Mississippi Valley-type mineralization: use of Sm–Nd in fluorite. Economic Geology 89, 1192–1199.

Claypool, G.E., Holster, W.T., Kaplan, I.R., Sakai, H., Zak, I., 1980. The age curves of sulphur and oxygen and their mutual interpretation. Chemical Geology 28, 199–260.

Clayton, R.N., O'Neil, J.R., Mayeda, T.K., 1972. Oxygen isotope exchange between quartz and water. Journal of Geophysical Research 77, 3057–3067.

Coleman, M.L., Moore, M.P., 1978. Direct reduction of sulphates to sulphur dioxide for isotopic analysis. Analytical Chemistry 50, 1594–1595.

Dunham, K.C., 1988. Pennine mineralization in depth. Proceedings of the Yorkshire Geology Society 47, 1–12.

Fernández, L.P., 1995. El Carbonífero. In: Aramburu, C., Bastida, F. (Eds.), Geología de Asturias, Gijón, pp. 63–81.

Gagnon, J.E., Samson, I.M., Fryer, B.J., Williams-Jones, A.E., 2003. Compositional heterogeneity in fluorite and the genesis of fluorite deposits: insights from IA-ICP-MS analysis. Canadian Mineralogist 41, 365–382.

Galindo, C., Tornos, F., Darbyshire, D.P.F., Casquet, C., 1994. The age and origin of the fluorite–barite (Pb–Zn) veins of the Sierra de Guadarrama (Eastern Iberian Central System): a radiogenic (Nd, Sr) and stable isotope study. Chemical Geology 112, 351–354.

García Iglesias, J., 1978. Estudio de inclusiones fluidas en los depósitos de fluorita de Berbes, Asturias. Boletín Geológico y Minero 89, 69–83.

García Iglesias, J., Loredo, J., 1992. Yacimientos de fluorita en Asturias. Recursos Minerales de España. Textos Universitarios. CSIC 15, 487–497.

García Iglesias, J., Loredo, J., 1994. Geological, geochemical and mineralogical characteristics of the Asturias fluorspar district. Exploration and Mining Geology 3, 31–37.

García Iglesias, J., Touray, J.C., 1976. Hydrocarbures liquides en inclusions dans la fluorite du gisement de La Cabaña, Berbes. Bulletin de la Société Française de Minéralogie et de Cristallographie 99, 117–118.

García Iglesias, J., Touray, J.C., 1977. A fluorite–calcite–quartz paragenesis with liquid and gaseous organic inclusions at La Cabaña, Berbes, Asturias fluorspar district, Spain. Economic Geology 72, 298–303.

Haas, J.R., Shock, E.L., Sassani, D., 1995. Rare earth in hydrothermal systems: estimates of standard partial molal thermodynamics of aqueous complexes of the rare earth elements at high pressures and temperatures. Geochimica et Cosmochimica Acta 21, 4329–4350.

Habitcht, K.S., Canfield, D.E., 1997. Sulfur isotope fractionation during bacterial sulfate reduction in organic-rich sediments. Geochimica et Cosmochimica Acta 61, 5351–5361.

Jørgensen, B.B., Isaksen, M.F., Jannasch, H.W., 1992. Bacterial sulfate reduction above 100 °C in deep-sea hydrothermal vent sediments. Science 258 (No. 5089), 1756–1757.

Kiyosu, Y., Krouse, H.R., 1990. The role of organic acid in the abiogenic reduction of sulfate and the sulfur isotope effect. Geochemical Journal 24, 21–27.

Koepnick, R.B., Denison, R.E., Burke, W.H., Hetherington, E.A., Dahl, D.A., 1990. Construction of the Triassic and Jurassic of the Phanerozoic curve of the seawater $^{87}Sr/^{86}Sr$. Chemical Geology 80, 327–349.

Kusakabe, M., Robinson, B.W., 1977. Oxygen and sulfur isotope equilibria in the $BaSO_4$–HSO_4–H_2O system from 110 to 350 °C and applications. Geochimica et Cosmochimica Acta 41, 1033–1040.

Loredo, J., Garcia Iglesias, J., 1984. Inclusions fluides et modèle génétique des minéralisations a fluorine dans le district Villabona–Arlós. Bulletin de Minéralogie 107, 217–226.

Lüders, V., Möller, P., 1992. Fluid evolution and ore deposition in the Harz Mountains (Germany). European Journal of Mineralogy 4, 1053–1068.

Ludwig, K.L., 1998. ISOPLOT/Ex, Version 1.00, a Geochronological Toolkit for Microsoft Excel: Berkeley Geochronology Center, Special Publication 1.

Machel, H.G., 2001. Bacterial and thermochemical sulfate reduction in diagenetic settings — old and new insights. Sedimentary Geology 140, 143–175.

McCrea, J.M., 1950. On the isotopic chemistry of carbonates and a paleotemperature scale. Journal of Chemical Physics 18, 849–857.

McLennan, S.M., 1989. Rare earth elements in sedimentary rocks: influence of provenance and sedimentary processes. Reviews in Mineralogy 21, 169–200.

Mizutani, Y., Rafter, T.A., 1969. Oxygen isotopic composition of sulphates. Part 3. Oxygen isotopic fractionation in the bisulphate ion–water system. New Zealand Journal of Science 12, 54–59.

Möller, P., Parekh, P.P., Schneider, H.J., 1976. The application of Tb/Ca–Tb/La abundance ratios to problems of fluorspar genesis. Mineralium Deposita 11, 111–116.

Möller, P., Morteani, G., Dulski, P., 1984. The origin of calcites from Pb–Zn veins in the Harz mountains, Federal Republic of Germany. Chemical Geology 45, 91–112.

Munoz, M., Premo, W.R., Courjault-Radé, P., 2005. Sm–Nd dating of fluorite from the worldclass Montroc fluorite deposit, southern Massif Central, France. Mineralium Deposita 39, 970–975.

O'Neil, J.R., Clayton, R.N., Mayeda, T.K., 1969. Oxygen isotope fractionation in divalent metal carbonates. Journal of Chemical Physics 51, 5547–5558.

Parekh, P.P., Möller, P., Dulski, P., 1977. Distribution of trace elements between carbonate and non-carbonate phases of limestone. Earth and Planetary Science Letters 34, 39–50.

Pfaff, K., Romer, R.L., Markl, G., 2009. U–Pb ages of ferberite, chalcedony, agate, U–mica and pitchblende: constraints on the mineralization history of the Schwarzwald ore district. European Journal of Mineralogy 21, 817–836.

Piqué, A., Canals, A., Grandía, F., Banks, D.A., 2008. Mesozoic fluorite veins in NE Spain record regional base metal-rich circulation through basin and basement during extensional events. Chemical Geology 257, 139–152.

Richard, P., Shimizu, N., Allègre, C.J., 1976. $^{143}Nd/^{144}Nd$ a natural tracer: an application to oceanic basalts. Earth and Planetary Science Letters 31, 269–278.

Richardson, C.K., Rye, R.O., Wasserman, M.D., 1988. The chemical and thermal evolution of the fluids in the Cave-in-Rock fluorspar district, Illinois: stable isotope systematics at the Deardoff mine. Economic Geology 83, 765–783.

Robinson, B., Kusakabe, M., 1975. Quantitative preparation of sulphur dioxide for $^{34}S/^{32}S$ analyses from sulphides by combustion with cuprous oxide. Analytical Chemistry 47, 1179–1181.

Sánchez de la Torre, L., Águeda-Villar, J.A., Colmenero, J.R., Manjón, M., 1977. La serie permotriásica en la región de Villaviciosa (Asturias). Cuadernos de Geología Ibérica 4, 329–337.

Sánchez, V., Corbella, M., Fuenlabrada, J.M., Vindel, E., Martín-Crespo, T., 2006. Sr and Nd isotope data from the fluorspar district of Asturias, Northern Spain. Journal of Geochemical Exploration 89, 348–350.

Sánchez, V., Vindel, V., Martín-Crespo, T., Corbella, M., Cardellach, E., Banks, D.A., 2009. Sources and composition of fluids associated with fluorite deposits of Asturias (N Spain). Geofluids 9, 338–355.

Sawkins, F.J., 1966. Ore genesis in the North Pennine ore field in light of fluid inclusions studies. Economic Geology 61, 385–401.

Schwinn, G., Markl, G., 2005. REE systematics in hydrothermal fluorite. Chemical Geology 216, 225–248.

Schwinn, G., Wagner, T., Baatartsogt, B., Markl, G., 2006. Quantification of mixing processes in ore-forming hydrothermal systems by combination of stable isotope and fluid inclusions analyses. Geochimica et Cosmochimica Acta 70, 965–982.

Sharp, Z.D., 1990. A laser-based microanalytical method for the *in situ* determination of oxygen isotope ratios of silicates and oxides. Geochimica et Cosmochimica Acta 54, 1353–1357.

Sizaret, S., Marcoux, E., Jebrak, M., Touray, J.C., 2004. The Rosignol fluoritevein, Chaillac, France: multiphase hydrothermal activity and intra-vein sedimentation. Economic Geology 99, 1107–1122.

Spirakis, C.S., 1991. The possible role of thiosulfate in the precipitation of ^{34}S-rich barite in some Mississippi Valley-type deposits. Mineralium Deposita 26, 60–65.

Tejerina, L., Zorrilla, J., 1980. Descripción geológica del distrito minero Caravia–Berbes (Asturias). Boletín Geológico y Minero 91 (6), 716–731.

Tornos, F., Delgado, A., Casquet, C., Galindo, C., 2000. 300 million years of episodic hydrothermal activity: stable isotope evidence from hydrothermal rocks of the Eastern Iberian Central System. Mineralium Deposita 35, 551–569.

Valverde, P., 1993. Permo-Carboniferous magmatic activity in the Cantabrian Zone (NE Iberian Massif, NW Spain). M.Sc Thesis, Boston College. Dpt. Geology and Geophysics, 498 pp.

Wood, S.A., 1990a. The aqueous geochemistry of the rare-earth elements and yttrium (1). Review of available low-temperature data for inorganic complexes and the inorganic REE speciation of natural waters. Chemical Geology 82, 159–186.

Wood, S.A., 1990b. The aqueous geochemistry of the rare-earth elements and yttrium (2). Theoretical predictions of speciation in hydrothermal solutions to 350 °C at saturation water vapor pressure. Chemical Geology 88, 99–125.